RESEARCH ARTICLE

Key Points:
- High-resolution foraminiferal Sr isotope record clearly shows precessional cyclicity
- Integrated model-data results indicate that late Miocene Sorbas Basin freshwater budget was positive
- Density contrast is a significant driver of interbasin exchange and thus Sr isotope anomalies

Precessional variability of ^{87}Sr/^{86}Sr in the late Miocene Sorbas Basin: An interdisciplinary study of drivers of interbasin exchange

Sevasti Modestou[1] (iD), Dirk Simon[2] (iD), Marcus Gutjahr[3] (iD), Alice Marzocchi[4,5] (iD), Tanja J. Kouwenhoven[2], Rob M. Ellam[1] (iD), and Rachel Flecker[4]

[1]SUERC, University of Glasgow, East Kilbride, UK, [2]Department of Earth Sciences, Utrecht University, Utrecht, Netherlands, [3]GEOMAR Helmholtz Centre for Ocean Research Kiel, Kiel, Germany, [4]BRIDGE, School of Geographical Sciences and Cabot Institute, University of Bristol, Bristol, UK, [5]Now at Department of the Geophysical Sciences, University of Chicago, Chicago, Illinois, USA

Abstract We present the first subprecessional record of seawater ^{87}Sr/^{86}Sr isotope ratios for a marginal Mediterranean subbasin. The sediments contained in this interval (three precessional cycles between 6.60 and 6.55 Ma) are important because they record conditions during the transition to the Messinian Salinity Crisis (MSC; 5.97 to 5.33 Ma), an event for which many details are still poorly understood. The record, derived from planktic foraminifera of the late Miocene Sorbas Basin (SE Spain), shows brief excursions with precessional cyclicity to ^{87}Sr/^{86}Sr ratios higher than coeval ocean ^{87}Sr/^{86}Sr. The hydrologic conditions required to generate the observed record are investigated using box modeling, constrained using a new paleodepth estimate (150 to 250 m) based on benthic foraminiferal assemblages. The box model results highlight the role of climate-driven interbasin density contrast as a significant driver of, or impediment to, exchange. The results are particularly significant in the context of the MSC, where ^{87}Sr/^{86}Sr excursions have been interpreted purely as a consequence of physical restriction. To replicate the observed temporal patterns of lithological variations and ^{87}Sr/^{86}Sr isotope excursions, the Sorbas Basin "box" must have a mainly positive hydrologic budget, in contrast with the Mediterranean's negative budget during the late Miocene. This result has implications for the assumption of synchronous deposition of specific sedimentary layers (sapropels) between marginal and open Mediterranean settings at subprecessional resolution. A net positive hydrologic budget in marginal Mediterranean subbasins may reconcile observations of freshwater inclusions in gypsum deposits.

Plain Language Summary Strontium isotopes in seawater can be used to investigate the connectivity of different bodies of water and their respective hydrologic budgets, two aspects which are very important for understanding paleogeography and climate in Earth's past. This paper uses numerical box modeling to investigate what a seawater Sr isotope record can tell us about one particular basin and its relationship to the Mediterranean Sea. Our findings indicate that the marginal basin investigated actually had a positive water budget at a time when the Mediterranean Sea was just about to undergo one of the most massive dessication events known in Earth's history, called the Messinian Salinity Crisis. Our findings also emphasize how important a lack of difference in densities in two water bodies can be as a barrier to water exchange. The conclusions have implications for how we understand communication between basins, but also help to improve our understanding of the timing of events on a very high temporal resolution, particularly at this relatively distant time in Earth's history (about 6 Myr ago).

1. Introduction

The Messinian Salinity Crisis (MSC) caused ~6% of global ocean salt to be sequestered on the floor of the Mediterranean Sea [*McKenzie*, 1999] in an evaporite layer ~1.5 km thick [*Hsü et al.*, 1973]. This extreme event was caused by restriction of the Miocene Atlantic-Mediterranean connections (Figure 1) as a result of tectonic uplift ranging from northern Morocco to Spain [*Krijgsman et al.*, 1999b, 2006] and eustatic sea level fall [*Manzi et al.*, 2013]. Much of our understanding of the conditions leading to the MSC and its timing is derived from astronomically tuned sequences exposed on the margins of the Mediterranean [e.g., *Krijgsman et al.*, 1999a; *Manzi et al.*, 2013]. Marginal sequences are used to infer Mediterranean Sea behavior because accessing deep-sea records is hindered by both the prohibitive expense and technical challenge of submarine
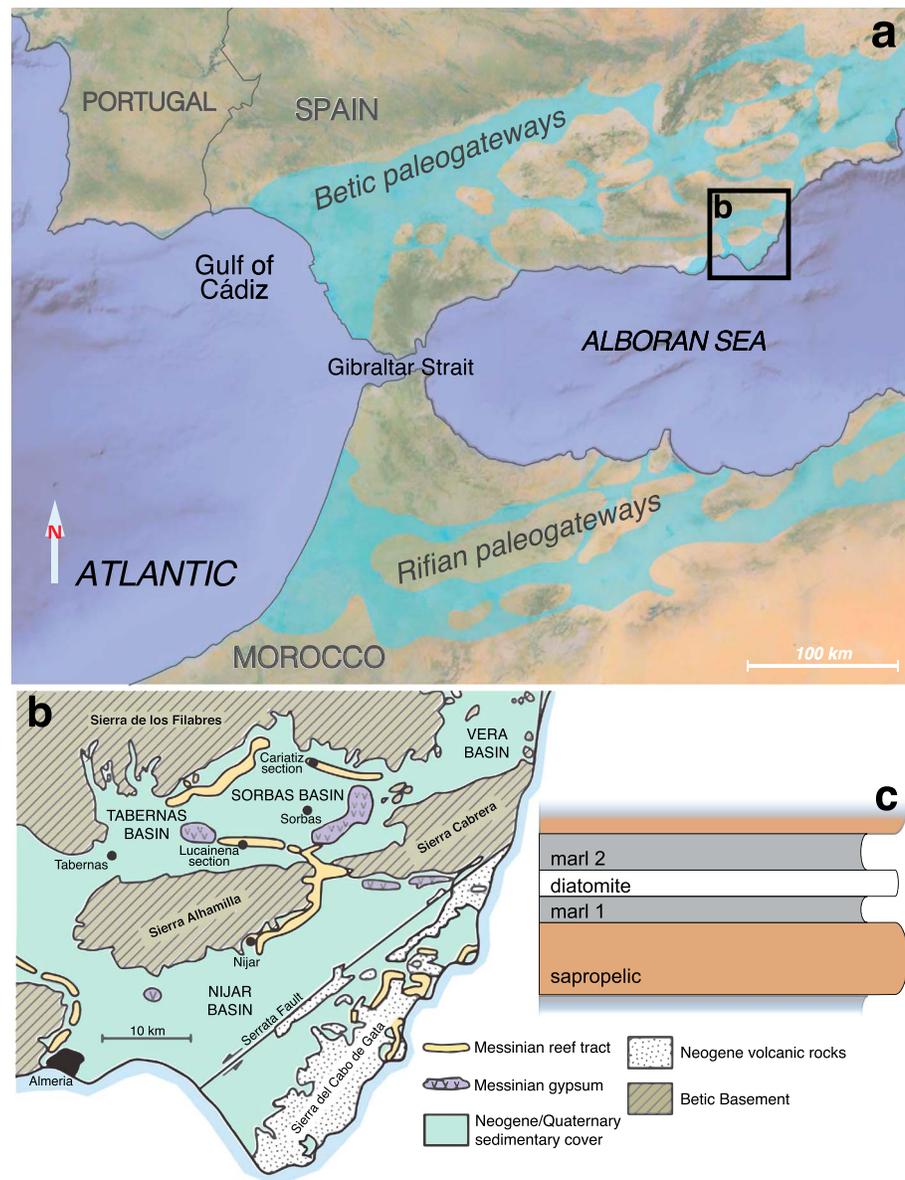
Figure 1. (a) The Sorbas Basin in the context of the Betic and Rifian paleogateways (light blue). Gateway configuration spans approximately 6–8 Ma (corridors closing through this period). The Gibraltar Strait is considered to have opened well after the paleogateways closed, at the Miocene-Pliocene boundary. Reconstruction of corridors based on *Santisteban and Taberner* [1983]. (b) Geological map of the Almería region; Neogene and Quaternary sedimentary cover coincides mainly with locations of paleogateways and basins. Modified from *Krijgsman et al.* [2001]. (c) Profile of Upper Abad quadripartite sedimentary cycle.

drilling through salt [*Roveri et al.*, 2014]. One way to test the validity of the underlying assumption that marginal basin and deep basin deposition were coeval is to use the marginal basin record to reconstruct exchange between marginal basins and the open Mediterranean and hence evaluate the likeliness of comparability of the two.

Many of the Mediterranean's Neogene marginal sedimentary records show strong precessional cyclicity. The sedimentary variation is thought to be a biogeochemical response to increased North African monsoonal precipitation during precession minima resulting in regular variations in freshwater discharge to the eastern Mediterranean [e.g., *Rossignol-Strick*, 1985; *Rossignol-Strick and Planchais*, 1989; *Larrasoaña et al.*, 2003; *Bosmans et al.*, 2015a; *Marzocchi et al.*, 2015]. Precessional variability in the Mediterranean's hydrologic budget has also been linked to changes in the velocity of Mediterranean outflow (MO) to the Atlantic

[*Bahr et al.*, 2015], suggesting that orbital changes in freshwater hydrology impact sedimentation and inter-basin exchange on precessional timescales.

Strontium isotopes are an elegant tool for investigating interbasin connectivity as they are sensitive to changing water sources. This tool has been used to reconstruct the connectivity of basins with limited connections to the open ocean on a variety of scales (e.g., Baltic Sea, San Francisco Bay, and Mississippi Delta [*Ingram and Depaolo*, 1993; *Andersson et al.*, 1994]) including the restriction of the Mediterranean from the Atlantic during the Messinian Salinity Crisis (MSC) [*Topper et al.*, 2011; *Roveri et al.*, 2014; *Schildgen et al.*, 2014; *Reghizzi et al.*, 2017]. Published pre-MSC Sr isotope records from some of the Mediterranean's marginal basins (i.e., Southern Turkey [*Flecker and Ellam*, 1999], the Adriatic [*Montanari et al.*, 1997], and Tyrrhenian Sea [*Müller and Mueller*, 1991]) deviate from global ocean Sr values up to 3.5 Myr before the first MSC evaporites were precipitated [*Flecker and Ellam*, 1999]. However, none of the records listed above have been astronomically tuned, either because they lack the sequence continuity required or because they include locally derived clastics which obscure orbital cyclicity. By contrast, coeval central Mediterranean records which have been tuned (e.g., Sicily [*Sprovieri et al.*, 2003], Cyprus [*Flecker and Ellam*, 2006], and Crete [*Flecker et al.*, 2002]) have oceanic ^{87}Sr/^{86}Sr values. Consequently, although there is clear evidence that some marginal Mediterranean basins have a profoundly different hydrologic budget from the main Mediterranean basin, none of the published Sr isotope records are of sufficiently high temporal resolution to evaluate marginal basin exchange with the open Mediterranean at subprecessional timescales.

The Sorbas Basin sediments in south-eastern Spain (Figure 1) have been astronomically tuned to precession [e.g., *Sierro et al.*, 1997, 1999; *Krijgsman et al.*, 2001] and are key successions for understanding the timing and behavior of the Western Mediterranean before and during the MSC, including being a crucial location for dating the onset of the MSC [*Krijgsman et al.*, 1999a; *Manzi et al.*, 2013]. Four pre-MSC sedimentary cycles from within the Sorbas Basin Abad Member have previously been studied at subprecessional resolution [see *Vázquez et al.*, 2000; *Filippelli et al.*, 2003; *Pérez-Folgado et al.*, 2003]. We analyzed fossil foraminifera from the same cycles to generate the first subprecessional temporal resolution Sr isotope record. To interpret this record, we apply box modeling to evaluate quantitatively the timing and nature of interbasin exchange and employ geochemical and environmental constraints from the previous studies to interpret the results of the model.

2. The Sorbas Basin

2.1. Sedimentology and Chronology

The Sorbas Basin lies at the eastern end of the Betic corridor, one of the two late Miocene gateways that connected the Mediterranean and Atlantic (Figure 1a). Although Mediterranean-Atlantic exchange through the Betic corridor likely ceased by ~7 Ma [*Esteban et al.*, 1996; *Martín et al.*, 2001, 2009; *Betzler et al.*, 2006], marine sedimentation persisted at its eastern and western ends. The Sorbas Basin marine marls of the Upper Abad (UA) Member were deposited from 6.71 Ma [*Sierro et al.*, 2001] until the onset of the MSC with precipitation of the Primary Lower Gypsum at 5.971 Ma [*Manzi et al.*, 2013]. The UA is characterized by repeating quadripartite cycles (Figures 1c and 2) [*Sierro et al.*, 1999, 2001, 2003], consisting of a brownish-grey laminated sapropelic layer; a bioturbated, homogenous grey marl ("marl 1"); diatomaceous marl ("diatomite"); and another grey homogenous marl ("marl 2"; Figures 1c and 2). These cycles are considered to be precessionally controlled [e.g., *Krijgsman et al.*, 1999a; *Sierro et al.*, 1999].

The UA sapropelic layers contain less total organic carbon [*Vázquez et al.*, 2000] than Plio-Pleistocene sapropels [e.g., *Murat*, 1999]. However, like sapropels, their formation has been linked to precession minima when enhanced monsoon-derived freshwater runoff stimulates productivity and reduced bottom water oxygenation (see *Rohling et al.* [2015] for an extensive review). Sediment laminations and the paucity of benthic foraminifera suggest that bottom water anoxia during precession minima is the primary control of sapropelic deposition in the Sorbas Basin [*Pérez-Folgado et al.*, 2003; *Sierro et al.*, 2003]. By contrast, the diatomite layer is thought to have formed during precession maxima, when drier conditions result in greater fresh water loss, higher surface water salinity, destabilization of the water column, and enhanced vertical mixing. These conditions cause nutrient upwelling and promote phytoplankton production. The homogeneous marl below the diatomite (marl 1; Figure 1c) likely marks the transition from sapropelic conditions to an environment with sufficient bottom water oxygenation to support benthic activity as laminations are no longer
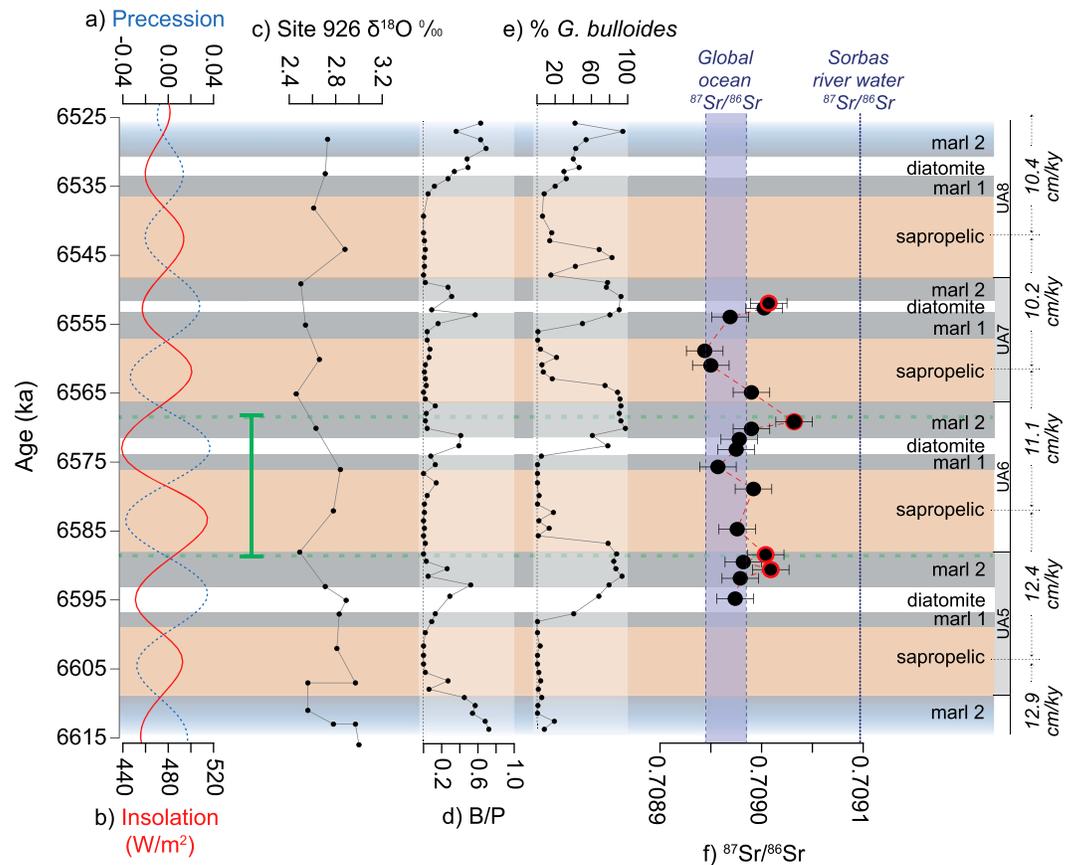
Figure 2. ^{87}Sr/^{86}Sr isotope compositions of Sorbas Basin water compared to lithology (Upper Abad marls, cycles UA5 to UA8), sedimentation rate (far right), and foraminifera data (foraminifera data tabulated in Table S5). (a) Precession and (b) insolation at 65°N [*Laskar et al.*, 2004]. (c) Ceara Rise (tropical W Atlantic) ODP Leg 154 Site 926 δ^{18}O [*Shackleton and Hall*, 1997]. (d) Sorbas basin B/P and (e) *G. bulloides* records from *Pérez-Folgado et al.* [2003]. (f) ^{87}Sr/^{86}Sr isotope compositions of Sorbas basin planktic foraminifera. Data points outside of analytical uncertainty of the global ocean ^{87}Sr/^{86}Sr curve are highlighted in red. Figures 2d–2f were generated from the same samples. The green bar indicates time span covered by GCM simulations.

preserved [*Sierro et al.*, 2003]. The transition from diatomite to marl 2 is thought to represent the depletion of nutrient-rich upwelling waters [*Sierro et al.*, 1999, 2003; *Filippelli et al.*, 2003].

Sedimentological observations and foraminiferal assemblages suggest that the basin was relatively shallow during the deposition of this member [*Troelstra et al.*, 1980; *Sierro et al.*, 1997; *Krijgsman et al.*, 2006]. However, existing depth estimates for the entire Abad Member range from 200 to 1000 m [*Dronkert*, 1976; *Troelstra et al.*, 1980; *Riding et al.*, 1998; *Poisson et al.*, 1999; *Baggley*, 2000], indicating a need for better constraints on paleobathymetry. Coeval fringing carbonate reefs [*Martín and Braga*, 1994; *Braga and Martín*, 1996] are used to constrain the basin's horizontal dimensions to ~40 × 30 km^2 (Figure 1b) (see geological maps of *Krijgsman et al.* [2001] and *Do Couto et al.* [2014]).

2.2. Sources of Sr

The interval covered by the data presented in this study spans 6.60–6.55 Ma. The average global ocean seawater ^{87}Sr/^{86}Sr at this time was 0.708965 ± 0.000020 [*McArthur et al.*, 2012], the mean changing only slightly from 0.708964 to 0.708966 over the interval. Because the concentration of Sr in seawater (8 mg/L) is more than an order of magnitude greater than in river water (global riverine average is 0.2 mg/L; up to ~0.5 mg/L for major rivers entering the Mediterranean [*Brass*, 1976; *Albarede and Michard*, 1987; *Palmer and Edmond*, 1989; *Reinhardt et al.*, 1998]), a measurable deviation from global ocean ^{87}Sr/^{86}Sr must be accompanied by a substantial increase in the source of nonmarine Sr relative to marine Sr. This is generally only observed in

very restricted marginal settings. The magnitude of riverine influx required to cause a Sr isotope anomaly also depends on the difference between the $^{87}Sr/^{86}Sr$ of the combining water masses. Both the Sr concentration ([Sr]) and isotope ratio of river water are controlled by catchment geology. Many European rivers entering the Mediterranean have catchments dominated by Mesozoic carbonate rocks with an $^{87}Sr/^{86}Sr$ composition lower than Miocene global ocean $^{87}Sr/^{86}Sr$ [*Flecker et al.*, 2002; *McArthur et al.*, 2012] and relatively high concentration (e.g., Rhone, 0.52 mg/L, $^{87}Sr/^{86}Sr$ 0.708719 [*Albarede and Michard*, 1987]). The Mediterranean's largest river, the Nile, has a basalt-dominated catchment which supplies very low $^{87}Sr/^{86}Sr$, although [Sr] is lower (0.235 mg/L, $^{87}Sr/^{86}Sr$ 0.7060 [*Brass*, 1976]). As a result the Sr anomalies observed across the Mediterranean in pre-MSC settings and during the MSC itself are dominated by deviations toward lower ratios than coeval ocean $^{87}Sr/^{86}Sr$ [*Flecker et al.*, 2015].

The $^{87}Sr/^{86}Sr$ of rivers feeding the Sorbas Basin during the Messinian can be constrained using published data from ostracods recovered from the lacustrine Zorreras member, located two units above gypsum deposited during the MSC and three units above the sediments studied here. The Zorreras member has a latest Messinian to earliest Pliocene age [*Martín and Braga*, 1994; *Fortuin et al.*, 1995; *Braga and Martin*, 1996; *Riding et al.*, 1998; *Roep et al.*, 1998; *Martin-Suarez et al.*, 2000; *Krijgsman et al.*, 2001; *Hilgen et al.*, 2007; *Aufgebauer and McCann*, 2010]. The Zorreras sediments are continental, although the ostracod-bearing levels are considered brackish water deposits [*Roep et al.*, 1998; *Aufgebauer and McCann*, 2010], suggesting that the ostracod-bearing levels represent either periodic ingress of seawater to the basin or an influence of dissolved salts from underlying deposits [*Roep et al.*, 1998; *Aufgebauer and McCann*, 2010]. Thus, the ostracod $^{87}Sr/^{86}Sr$ ratios should provide a conservative minimum estimate for Sorbas river water Sr isotope compositions, as they should fall below the true riverine Sr isotope value due to the influence of oceanic Sr. The ostracods have an $^{87}Sr/^{86}Sr$ ranging from 0.709066 to 0.709131 (average = 0.709097; $n = 4$ [*McCulloch and De Deckker*, 1989], originally published in *Roep and van Harten* [1979]). These values are higher than coeval ocean water values and are consistent with the high Sr isotope values anticipated from the catchment. Since the individual values are derived from only one ostracod valve, rather than a large number of individuals as is customary for foraminiferal $^{87}Sr/^{86}Sr$ data, we have chosen to use the average to represent Sorbas Basin water overall.

The Internal Betic Cordillera of SE Spain contains rocks with higher Sr isotopic ratios than late Miocene ocean water [*Powell and Bell*, 1970; *Hebeda et al.*, 1980; *Zeck et al.*, 1989; *de Jong*, 2003; *Conticelli et al.*, 2009]. The Sierras surrounding the Sorbas Basin (Figure 1b) form the eastern end of this Cordillera. The fine-grained nature of the Abad Marls impedes provenance analysis; however, clasts derived from the Sierras are found within the underlying Azagador Member [*Braga et al.*, 2001] and the overlying Zorreras Member [*Aufgebauer and McCann*, 2010] [see *Krijgsman et al.*, 2001, Figure 2]. Available evidence for the Sierra de los Filabres, the range bounding the Sorbas Basin to the North (Figure 1b), indicates that exhumation due to rock (not surface) uplift stopped before the Messinian (~ 8 Ma [*Vazquez et al.*, 2011]), suggesting that drainage network reorganization exposing significantly different geology is unlikely to have occurred between deposition of the sediments investigated in this study and deposition of the ostracods. Regional volcanic rocks, emplaced during the late Miocene, are also characterized by $^{87}Sr/^{86}Sr$ higher than coeval ocean water ratios [*Toscani et al.*, 1990; *Benito et al.*, 1999; *Duggen et al.*, 2008; *Conticelli et al.*, 2009]. If this volcanism affected the Sorbas Basin, it would also have produced an $^{87}Sr/^{86}Sr$ signature higher than coeval ocean water.

The concentration of Sr in river water correlates with the mineralogy of the catchment; carbonate-rich drainage basins tend to exhibit higher concentrations, around ~0.5 mg/L. In comparison, catchments dominated by siliciclastic rocks tend to have lower [Sr] [e.g., *Blum et al.*, 1998; *English et al.*, 2000; *Jacobson and Blum*, 2000]). Considering the primarily noncarbonate catchment and the lack of direct measurements on modern day analogs, we have based our river [Sr] estimate from both basic and acidic terrains summarized by *Brass* [1976] (0.25 mg/L) and added 0.05 mg/L to account for the presence of some carbonate rocks. Thus, we employ [Sr] = 0.3 mg/L as a maximum estimate for water flowing into the Sorbas Basin in the late Miocene. Implications for a range (0.1 to 0.5 mg/L) of [Sr] are also addressed.

3. Methodology

3.1. Age Model

The precessional-resolution stratigraphic framework for the Abad Formation is based on integrated biostratigraphy, magnetostratigraphy, and cyclostratigraphy [*Krijgsman et al.*, 1999a, 2001, *Sierro et al.*, 1999, 2003]. A

limitation of cyclostratigraphy is the uncertainty in the phase relationship between sedimentation, climate, and insolation. For Mediterranean deposits, in general, *Lourens et al.* [1996] determined an ~3 kyr lag from precession minima to the midpoint of the youngest eastern Mediterranean sapropel, S1, based on ^{14}C dating; this lag was hypothesized to be the time required for climate to respond to changes in solar insolation [*Lourens et al.*, 2004]. By contrast, a model study by *Weber and Tuenter* [2011] determined that little to no time lag exists for precessional climate forcing, particularly at midlatitudes. Specifically for the Abad marls of the Sorbas Basin, *Pérez-Folgado et al.* [2003] proposed that deposition of the sapropelic layers coincided with the transition from precession maxima to precession minima, based on a comparison of faunal responses measured at subprecessional resolution in the Sorbas Abad marls and an open Mediterranean site (Gavdos). While the cyclicity of changes in foraminiferal assemblages is essentially identical at the two locations, the lithological cyclicity is not. As the correct precession-lithology phasing is still unclear, we followed *Krijgsman et al.* [1999a] and assigned peaks in precession minima to the midpoints of sapropelic layers, assuming constant sedimentation rates between midpoints. The astronomical tuning from *Krijgsman et al.* [1999a] has been updated to La04 [*Laskar et al.*, 2004] using summer insolation at 65°N (see *Lourens et al.* [1996] for justification). Age uncertainty is not estimated, as the relative spatiotemporal relationship between the sediment layers and faunal or isotope data are both more precise and significant than absolute age for our study.

3.2. Foraminiferal [87]Sr/[86]Sr

Samples from the lower interval of the UA marls (cycles UA5 to UA8, ~6.61 to 6.55 Ma, [*Sierro et al.*, 2001]) were collected from an ~10 m section near Los Molinos (37°05′22″N, 2°04′08″W) for high temporal resolution studies [see *Filippelli et al.*, 2003; *Pérez-Folgado et al.*, 2003]. Surface material was removed before collecting fresh, uncontaminated sediment (F. Sierro, personal communication).

A minimum of 100 mixed planktic foraminifera (primarily *Orbulina universa* and *Globigerina* spp.) were picked from disaggregated and washed samples (see *Pérez-Folgado et al.* [2003] for details) following well-established methods [e.g., *Barker et al.*, 2003; *McArthur et al.*, 2006; *Schildgen et al.*, 2014]. Preservation was checked visually during picking under a binocular microscope; only tests devoid of signs of calcite infilling or encrustation, or significant recrystallization, were selected. Foraminiferal tests were gently crushed to break open each chamber, and material within chambers was removed. In acid-cleaned 1.5 mL centrifuge tubes, samples were subjected to repeated ultrasonification in ≥18.2 MΩ deionized water, once in ethanol, and again in deionized water. The liquid from each step was removed by pipette, ensuring the final water rinse before the ethanol step was clear and free from clays. Test fragments were reexamined under the microscope after the cleaning process, and any fragments with visible signs of contamination were rejected. Samples were leached in 1 M ammonium acetate for 1 h to remove easily exchangeable Sr [*Melezhik et al.*, 2001, and references therein] and ultrasonicated a further three times in deionized water. Cleaned calcite was digested in 5% acetic acid with ultrasonification for a maximum of 10 min. Residue was separated by centrifugation and the supernatant dried and converted to nitrate form with 200 μL concentrated HNO_3. Sr was separated using standard column chromatography on Eichrom Sr spec resin following *Henderson et al.* [1994]. The potential effects of diagenesis are considered in detail in section S4 in the supporting information [*Beets and De Ruig*, 1992; *Flecker et al.*, 1998; *Richter and Liang*, 1993; *Baker et al.*, 1982; *Richter and Liang*, 1993; *Voigt et al.*, 2015].

Isotope analysis was performed with a VG Sector 54-30 multiple collector thermal ionization mass spectrometer at Scottish Universities Environmental Research Centre (East Kilbride, UK). Samples were loaded onto single Re filaments with a Ta-activator similar to that described by *Birck* [1986]. An [88]Sr intensity of ~1 × 10^{-11} A ± 10% was maintained. [87]Sr/[86]Sr was corrected for mass fractionation to [86]Sr/[88]Sr = 0.1194 [*Nier*, 1938] using an exponential law. The mass spectrometer was operated in dynamic mode with data collected in 15 blocks of 10 ratios. Procedural blanks, introduced after the foraminifera crushing stage, were <0.16 ng Sr, contributing less than 0.05% to sample mass. National Institute of Standards and Technology Standard Reference Materials 987 gave 0.710259 ± 0.000018 (2 SD, *n* = 24) during the course of the analyses. The 2 standard error internal precision on individual analyses ranged between 12 and 17 ppm (smaller than external reproducibility).

3.3. Box Model Setup and Parameter Selection

Numerical box modeling was used to provide quantitative constraints on the hydrologic budget and interbasin exchange required to reproduce our Sr data. Earlier work [e.g., *Flecker et al.*, 2002; *Meijer*, 2006; *Topper et al.*,

Table 1. Summary of Constraints Used for Box Modeling

Parameter	Value	References and Notes
	Sorbas Basin Geometry	
Surface area	1.2×10^9 m^2	*Krijgsman et al.* [2001]; *Do Couto et al.* [2014]
Depth	200 m	Benthic foraminiferal assemblages, this study; for depth sensitivity test results; see Text S3
Volume	2.4×10^{11} m^3	Calculated, surface area × depth
Sr Concentration		
Mediterranean	8 mg/L	*Veizer* [1989]
Sorbas basin	8 mg/L (initial)	
River	0.3 mg/L (0.1–0.5 mg/L considered)	text, section 2.2
	^{87}Sr/^{86}Sr *Isotope Ratios*	
Mediterranean	0.708965	*McArthur et al.* [2012]
River	0.709097	text, section 2.2
Anomaly	0.709003	text, section 3.3
Salinity		
Mediterranean	37 g/L	text, section 3.3
Sorbas basin	30–49 g/L	
River	0 g/L	
	Sorbas Hydrologic Budget	
Evaporation (E)	41.77–43.27 m^3/s	*Marzocchi et al.* [2016]; Table S1
Precipitation (P)	8.85–12.11 m^3/s	(minimum-maximum value; annual means)

2011, 2014] coupled mass balance equations for water, salinity, and ^{87}Sr/^{86}Sr to examine the Sr isotope and salinity evolution and constrain exchange for the Messinian Mediterranean. We use a similar approach to explore the impact of the hydrologic budget and interbasin exchange on the ^{87}Sr/^{86}Sr signatures and focus on regions of the box model results that correspond to our Sr isotope data. Steady state estimates provide useful insight for a basin which adjusts very quickly to inputs. Here steady state solutions provide estimates of the fluxes of inflow (Q_I), outflow (Q_O), and river water (Q_R) as well as the evaporation (E) and precipitation (P), required to effect change in the ^{87}Sr/^{86}Sr of the basin while maintaining appropriate salinities. The sum of the exchange (Q_I and Q_O) and the Sorbas freshwater budget (Q_R, E, and P) is defined as the hydrologic budget of the Sorbas basin (section S1). Transient solutions are required to assess the time required to reach a Sr isotope anomaly and to investigate the dynamic temporal evolution of hydrologic budget parameters. Several parameters must be estimated to enable modeling of the system. Available and assumed constraints used are summarized in Table 1. Equations are detailed in the supporting information, alongside further justification of parameter selection.

Only Sorbas Sr isotopic compositions that fall outside the coeval global ocean range are considered anomalous (0.708965 ± 0.000020; see Text S5 in the supporting information for treatment of the Sr isotope ocean curve and the derivation of the uncertainty [*Farrell et al.*, 1995; *Martin et al.*, 1999]). Considering the analytical uncertainty of our data (0.000018), the minimum anomalous ^{87}Sr/^{86}Sr value above coeval ocean water values is 0.709003. The Sorbas Basin surface area is estimated from its paleogeography (section 2.1), and the depth is estimated from new benthic foraminifera data (see section 4.2 and Table S4 in the supporting information). Planktic foraminifera are present throughout the entire interval [*Pérez-Folgado et al.*, 2003], indicating that salinity in the Sorbas Basin never exceeded 49 g/L [*Fenton et al.*, 2000] during this interval. Faunal assemblages reported here (Table S4) and published previously [*Pérez-Folgado et al.*, 2003; *Sierro et al.*, 2003] also show that the basin did not experience brackish conditions. Although laboratory experiments have shown that some species of planktic foraminifera can thrive at salinities as low as ~25 g/L [*Bijma et al.*, 1990], the atlas of *Hillbrecht* [1996] indicates that the natural abundance of extant planktic foraminifera drops to zero between 32 and 33 g/L. Based on these estimates, we employed a minimum salinity threshold of 30 g/L. The salinity of the Sorbas "box" must therefore remain within the range 30 to 49 g/L for model results to be considered compatible with the presence of planktic foraminifera. Mediterranean salinity adjacent to the Sorbas Basin is assumed to be 37 g/L which is the average salinity of the present-day Alborán Sea (Figure 1a) [*Levitus et al.*, 1994]. The upper water mass in the Alborán Sea consists of Atlantic water which has been partially mixed with Mediterranean Outflow [*Millot*, 1999]; consequently, the westernmost

Mediterranean has experienced smaller changes in salinity than the rest of the Mediterranean basin over the past 16,000 years [*Emeis et al.*, 2000]. We therefore assume constant Western Mediterranean salinity and explore the sensitivity of the model to this selection.

Values for the freshwater budget terms E and P are derived from global general circulation model (GCM) simulations using UK Hadley Centre Coupled Model version 4.5. Twenty-two steady state snapshot simulations at 1 kyr intervals were distributed over a real precessional cycle between 6.589 and 6.568 Ma [*Marzocchi et al.*, 2015] spanning most of cycle UA6 (green bar, Figure 2). The orbital solution of *Laskar et al.* [2004] was used to determine the orbital parameters for each snapshot simulation to capture the complete orbital variability. The full experimental design is published in *Marzocchi et al.* [2015]. The values of P and E for both the western and eastern Mediterranean basins from each simulation are shown in Table S1 (values for the full Mediterranean Sea are discussed in *Marzocchi et al.* [2016]; see their Figure 1b). We used maximum and minimum annual means for the Western Mediterranean (Table S1), scaled to the surface area of the Sorbas Basin. We employed a sine function to vary between the hydrologic budget extremes over 20 kyr cycles, similarly to *Topper et al.* [2014].

The box model consists of one box representing the Sorbas Basin, connected to a "basin" with constant conditions representing the western Mediterranean (Figure S1 in the supporting information). The only significant deviation from *Topper et al.* [2011] is the introduction of a Sr concentration limit at 8 mg/L; this is the ocean water [Sr] [*Veizer*, 1989] and essentially represents the solubility limit of Sr in seawater of normal marine salinity. Imposing this limit prevents the model from generating artificially high [Sr] not representative of the natural environment and results in the riverine Sr input having greater impact on the basin's Sr isotope ratio. With respect to the Sorbas Basin box, the impact is very small. In systems with larger differences between seawater and riverine Sr isotope ratios, or greater riverine [Sr] than that assumed for the Sorbas Basin here, the impact of this solubility limit may be quite significant. Sr precipitation and deposition are ignored, as these processes do not affect basin connectivity or basin water $^{87}Sr/^{86}Sr$.

The GCM simulations indicate that most of the variability in the Western Mediterranean's freshwater budget is driven by P (section S2 and Table S1), which appears to be driven by precessional changes in the Atlantic winter storm tracks [e.g., *Kutzbach et al.*, 2014], suggesting that riverine runoff (Q_R) should also vary with precession. However, we have used a constant Q_R for each box model simulation and varied the hydrologic budget using variables E and P. Since Q_R is the only freshwater flux that also delivers Sr to the basin, constant Q_R simplifies the temporal changes in Sr mass flux to the basin. This selection makes the results easier to interpret but requires justification. Sensitivity to this selection was explored by comparing model results (not shown) with the same overall freshwater budget, achieved by varying either E, P, Q_R, or various combinations of these terms. The range of $^{87}Sr/^{86}Sr$ and salinities resulting from these tests were very similar regardless of which freshwater budget parameter(s) varied. This is probably because the range of values for P, or the combined EP term, is relatively small (P = 8.85 to 12.11 m^3/s, EP = 30.48 to 33.16 m^3/s). Consequently, although varying Q_R with precession is more realistic, it was kept constant for any one model run. For systems with larger expected variation in P, this choice may not be justified.

For both steady state and transient simulations, salinity is assumed to be an adequate approximation for density as per *Meijer* [2006]. The linear exchange coefficient g expresses gateway efficiency, where g = 1 m^3/s per g/L indicates a very inefficient gateway. This value is relevant for transient simulations (section S1, equation 3). Low values of g can be related to small gateway dimensions (such as narrow, long, or tortuous gateways; see *Simon and Meijer* [2015] for discussion of the impact of gateway dimensions on exchange). No estimate of g is available so we use the model to find the range of g values consistent with periodic $^{87}Sr/^{86}Sr$ anomalies. To determine optimum values of Q_R and g, the transient model was run for a large range of Q_R and g in order to predict the optimal combinations required to generate a Sr anomaly (from 29 to 35 m^3/s for Q_R and from 0.5 to 250 m^3/s per g/L for g; note that only ranges which generate anomalies are shown).

It should be noted that our box modeling requires the assumption that the global ocean Sr isotope curve does not vary with precession, an assumption used previously [e.g., *Schildgen et al.*, 2014; *Topper et al.*, 2014]. The ocean $^{87}Sr/^{86}Sr$ curve for this interval is based on data with approximately 15 kyr resolution; thus, unresolved variability at shorter timescales may exist. However, variability of ocean $^{87}Sr/^{86}Sr$ on precessional timescales would require very significant precessional changes in global weathering patterns. During major

changes in weathering such as Northern Hemisphere glacial–interglacial cycles, cyclicity in ocean $^{87}Sr/^{86}Sr$ is not observed [see, for example, *Vance et al.*, 2009, Figure 4]. This is primarily due to the long residence time of Sr and the high [Sr] in seawater compared to continental runoff. Consequently, precessional variability in the global ocean Sr isotope record is unlikely.

3.4. Benthic Foraminiferal Assemblages

Paleobathymetric estimates can be derived from the benthic to planktic foraminifera ratio (B/P), where deeper water is reflected in lower ratios [*Van der Zwaan et al.*, 1990]. However, benthic foraminifera are sensitive to bottom water oxygenation, and during extended periods of anoxia, sediments can become completely devoid of these bottom-dwellers, irrespective of basin depth. Because of the cyclical pattern of bottom water anoxia in the UA marls, B/P cannot be used to determine the paleobathymetry of the Sorbas Basin [*Van Hinsbergen et al.*, 2005]. Benthic foraminiferal assemblages, however, can provide constraints on paleodepth, as well as more specific information about bottom water conditions. Twelve samples spanning UA5–7 were counted for benthic foraminifera species (Table S4).

4. Results

4.1. Sorbas Sr Isotopic Compositions

All but four of the measured $^{87}Sr/^{86}Sr$ values are within error of the coeval global seawater curve (Figure 2f and Table S3). These four anomalous Sr isotope ratios all have higher ratios than coeval seawater and occur in the nonsapropelic layers, within the diatomites or the immediately following homogenous marl (Figure 2). The Sr anomalies occur coevally with maxima in the percentage of *Globigerina bulloides* (Figure 2e). The Sr anomalies are also consistently preceded by elevated B/P (Figure 2d). Both faunal oscillations, like the regular lithological change, are thought to fluctuate with insolation [*Pérez-Folgado et al.*, 2003; *Sierro et al.*, 2003] (Figure 2). Due to the regular pattern of Sr isotope anomalies, we suggest that the foraminifera $^{87}Sr/^{86}Sr$ is largely unaffected by diagenetic alteration.

4.2. Sorbas Paleodepth and Bottom Water Oxygenation

The benthic foraminiferal assemblages found in marls 1 and 2 are indicative of shelf edge or outer shelf conditions and suggest a water depth range of approximately 150–250 (mean ~ 200) m (Table S4). Our estimate is in good agreement with *Troelstra et al.* [1980], who suggested that the UA marls experienced shallowing from about ~200 m water depth at the base of the section to ~100 m near the top. Our estimate is specifically applicable to cycles UA5 to 8 in the lower part of the UA and is based on species shaded in Table S4. Species restricted to inner shelf or coastal environments (such as *Ammonia* and *Elphidium* spp. [e.g., *Alve and Murray*, 1999]) are subordinate or absent. For most other benthic species depth distributions are not fixed [e.g., *Wright*, 1978; *De Rijk et al.*, 2000]. However, of the species shaded in Table S4, *Cibicides lobatulus*, *C. pachyderma*, *C. ungerianus*, and *Planulina ariminensis* occur and *Cassidulina laevigata*, *Hanzawaia boueana*, *Nonion fabum*, and *Valvulineria bradyana* are most abundant in shelf environments [e.g., *Schmiedl et al.*, 1997; *De Stigter et al.*, 1998; *Licari and Mackensen*, 2005; *Mojtahid et al.*, 2009; *Dorst and Schönfeld*, 2013].

The majority of the sapropelic samples contain no benthic foraminifera (Figure 2d) [*Pérez-Folgado et al.*, 2003, Figures 2b and 2c]. Our analysis indicates that when benthic foraminifera are present, even while they comprise a relatively high percentage of the overall foraminiferal assemblage, the populations are dominated by stress-tolerant species (*Bolivina*, *Bulimina*, (*Rect-*) *Uvigerina*, and *Globobulimina* spp.) indicative of hypoxic conditions [*Kouwenhoven et al.*, 2003; *Van Hinsbergen et al.*, 2005; *Koho et al.*, 2011; *Koho and Piña-Ochoa*, 2012; *Langlet et al.*, 2014]. Stress tolerant species percentages range from 40% to 100%, with the majority of samples containing more than 50%. This systematic pattern of benthic foraminifera occurrence suggests that during sapropelic layer deposition anoxia was extreme enough to prevent benthic foraminifera survival, while during marl and diatomite deposition anoxia lessened to hypoxic conditions. For the marl and diatomite layers, the B/P therefore indicates episodes of increased seafloor oxygenation where the most oxygenated conditions commonly immediately precede the Sr anomalies (Figures 2d and 2f).

4.3. Model Results
4.3.1. Steady State Box Model Results

For the Mediterranean Sea, *Topper* [2013] calculated that at least 25% of the water flux into the basin during the late Miocene must be riverine to generate a measureable Sr anomaly; e.g., a $Q_R:Q_I$ ratio of ~1:3. Assuming
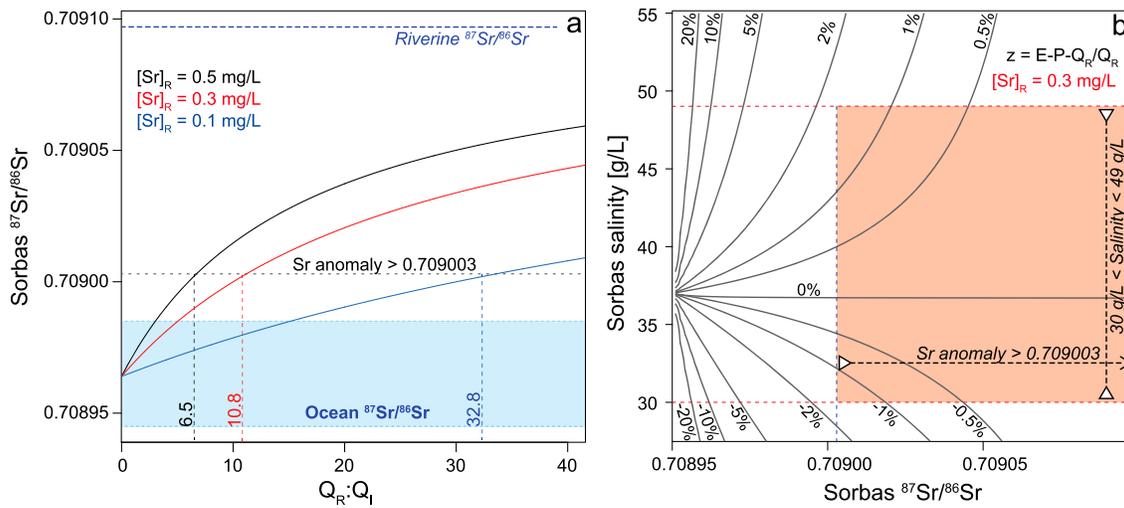
Figure 3. Steady state model results. (a) Sorbas Basin Sr isotope ratio ([^{87}Sr/^{86}Sr]$_S$) versus $Q_R{:}Q_I$ for riverine Sr concentrations ([Sr]$_R$) from 0.1 to 0.5 mg/L. The values on vertical lines indicate minimum $Q_R{:}Q_I$ for an anomaly to occur for each river water [Sr]. (b) Contour plot of $(E - P - Q_R)/Q_R$, with respect to Sorbas Basin salinity and ^{87}Sr/^{86}Sr, using [Sr]$_R$ = 0.3 mg/L. Sr anomaly requires $Q_R = E - P \pm {\sim}1.7\%$, as indicated by shaded box.

that the ^{87}Sr/^{86}Sr of Nile runoff was similar to today, this implies a 2965 ppm difference between the late Miocene global ocean ^{87}Sr/^{86}Sr and that of the freshwater source dominating the runoff to the Mediterranean. At the midpoint of the interval studied here, the estimated late Miocene Sorbas fluvial Sr isotope ratio (Table 1) differs from the global ocean value by only 132 ppm; thus, a larger $Q_R{:}Q_I$ ratio is required to generate a measureable Sr anomaly. Assuming riverine Sr concentrations of 0.5 mg/L, 0.3 mg/L, and 0.1 mg/L, the $Q_R{:}Q_I$ ratios required to observe a Sr isotope anomaly in the Sorbas Basin are 6.5:1, 10.8:1, and 32.8:1 respectively (Figure 3a). In order to attain a Sr isotope anomaly while maintaining a salinity suitable for foraminifera, for [Sr]$_R$ = 0.3 mg/L, Q_R must be very small, i.e., $Q_R \leq E - P \pm 1.7\%$, or within 1.7% of a neutral freshwater budget (Figure 3b).

Combining these results with minimum and maximum E and P from the GCM data (Table S1) allows us to calculate an expected range of river runoff (Q_R) into the basin for the salinity range required. For [Sr]$_R$ = 0.5 mg/L, Q_R = 29.6 to 34.2 m^3/s; for lower concentrations, the range narrows slightly ([Sr]$_R$ = 0.3 mg/L, Q_R = 30.0 to 33.8 m^3/s; [Sr]$_R$ = 0.1 mg/L, Q_R = 30.3 to 33.4 m^3/s). These ranges in discharge are comparable with the annual discharge for small modern rivers in Southern Spain such as the Segura (~ 26 m^3/s, SAGE database; compare with the Ebro ~429 m^3/s at Tortosa, the Nile ~1254 m^3/s at El Ekhsase, or the Rhône ~1712 m^3/s at Beaucaire, SAGE database). The modeled runoff values are an estimate for the entire basin and thus represent the total from multiple sources. Thus, the low discharge predicted by our box model is consistent with the absence of large-scale deltaic or fluvial deposits in the pre-MSC successions of the Sorbas Basin. The only clastic deposits similar in age to our interval reported in the literature are from the Lucainena section (Figure 1b) [*Sanchez-Almazo et al.*, 2001]. The Rio de Aguas, the main river draining the Sorbas Basin today, has a median annual discharge of only ~1 m^3/s [*Pulido-Bosch*, 1997], although significant catchment reorganization is suspected during the early Pleistocene, leading to diversion of water to other areas [*Mather*, 2000].

4.3.2. Transient Model Results

The combinations of the linear exchange coefficient g and riverine influx Q_R capable of generating a Sr isotope anomaly in the transient model are shown in Figure 4a. There are only two cases which produce Sr isotope anomaly patterns similar to the data: (1) when the freshwater budget is mainly positive and approaches neutral or briefly becomes negative once per cycle (Figure 4b) and (2) when the freshwater budget is mainly negative and approaches neutral or briefly becomes positive once per cycle (Figure 4d). The freshwater budget must remain either positive ($E < P + Q_R$) or negative ($E > P + Q_R$) throughout the majority of a precessional cycle in order to correctly generate a single Sr ratio anomaly "peak" per cycle (Figure 2f). Where the freshwater budget becomes neutral twice per cycle (e.g., the freshwater
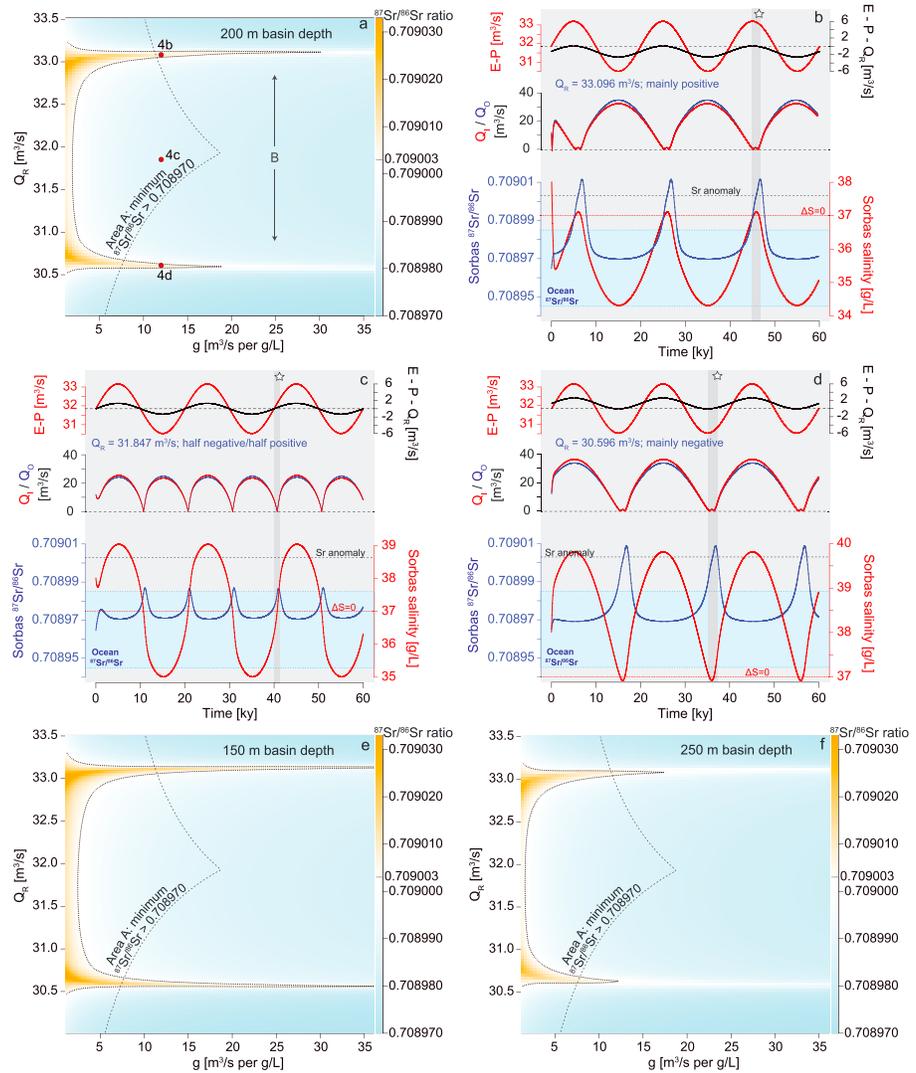
Figure 4. Transient model results. (a) Contour plot (200 m basin depth) for Q_R and g parameter space generating a Sr isotope anomaly; the orange areas (outlined by dotted line) indicate peak $^{87}Sr/^{86}Sr > 0.709003$. Area A: values of Q_R and g that do not allow minimum (between-peak) $^{87}Sr/^{86}Sr$ to return to global ocean value (allowing for 5 ppm margin above the seawater value, up to $^{87}Sr/^{86}Sr = 0.708970$); Sr isotope anomalies are observed in this region, but the foraminifera data pattern is not reproduced (Figure 2). Area B (space between anomaly regions): insufficient time near neutral hydrologic budget to generate an anomaly. (b–d) Time series for Q_R and g combinations indicated in Figure 4a. Hydrologic budgets (upper curves), evolution of Q_I and Q_O (middle curves), basin salinity, and $^{87}Sr/^{86}Sr$ (lower curves); $g = 12$ m^3/s per g/L for all time series (this value of g was selected as it generates easily visible anomalies, and maintaining the same g throughout means that only one parameter is changing in the time series plots making the relationships easier to understand; however, $7.4 < g < 33.5$ m^3/s per g/L can generate an anomaly at this basin depth/volume). $\Delta S = 0$: Sorbas and Mediterranean salinities equal. Sr anomaly: minimum observable $^{87}Sr/^{86}Sr$ anomaly (≥ 0.709003; section 3.3). Freshwater budgets vary cyclically through minimum and maximum $E - P$ over 20 kyr to generate mainly positive (average $E < P + Q_R$) (Figure 4b), half positive/half negative (average $E = P + Q_R$; Figure 4c), and mainly negative (average $E > P + Q_R$) hydrologic budgets (Figure 4d). Positive freshwater budget axe values indicate freshwater loss, as the term ($E - P - Q_R$) is positive in the model (see the supporting information). The star-marked bars emphasize small time lag between peak hydrologic budget values, salinity, and $^{87}Sr/^{86}Sr$. (d–f) Peak $^{87}Sr/^{86}Sr$ encountered over a 20 kyr model cycle for given g and Q_R. (e and f) Contour plots illustrating model sensitivity to basin depth. Q_R and g combinations employed for Figures 4b–4d are indicated by red dots.

budget is positive for half a cycle and negative the other half, so that on average $E = P + Q_R$; Figure 4c), two ^{87}Sr/^{86}Sr peaks occur per precessional cycle. The peaks produced in the latter case are also analytically indistinguishable from ocean water.

Area A (Figure 4a), the region where Sr isotope ratios do not return to global ocean values between anomalies, reduces the range of Q_R and g values which satisfy the requirement to reproduce the data. A 5 ppm tolerance on the ocean water ^{87}Sr/^{86}Sr value was added, such that values above 0.708970 at ^{87}Sr/^{86}Sr minima are considered not representative of the foraminifera data (Figure 2f). The Q_R values between the two regions of Sr isotope anomalies (Area B; Figure 4a) are not anomalous due to insufficient time near a neutral fresh water budget ($\Delta S = 0$). The specific ranges of Q_R and g values which reproduce the data are g from 11.3 to 33.5 m^3/s per g/L and Q_R from 33.05 to 33.13 m^3/s (positive hydrologic budget case, e.g., Figure 4b) and g from 7.4 to 24.2 m^3/s per g/L; Q_R from 30.57 to 30.67 m^3/s (negative hydrologic budget case, e.g., Figure 4d). The narrow Q_R ranges are a result of the time that a state near $\Delta S = 0$ must be maintained to generate an anomaly and the sensitivity of salinity in a small basin to freshwater fluxes. The absolute values of the Sorbas-Mediterranean exchange coefficient, g, are small by comparison with the modern Gibraltar strait ($\sim 10^5$ m^3/s per g/L), and the g required at Gibraltar to cause measureable changes in Mediterranean Sr isotope ratios ($<10^3$ m^3/s per g/L) [Topper et al., 2011]. The range of g, however, is wide compared to the range of Q_R values; this is because as ΔS approaches zero, the Q_I and Q_O exchange fluxes approach zero, irrespective of gateway efficiency.

The lack of salinity difference between the basins acts as a barrier to exchange, similarly to a physical blockage in the gateway (addressed further, sections 5.1.2 and 5.2). This is because the exchange between basins is driven by density difference. Modern exchange at Gibraltar provides an analogy on the significance of the density-contrast mechanism, where exchange increases proportionally with the density difference between Mediterranean and Atlantic water [e.g., Bryden and Stommel, 1984; Bryden and Kinder, 1991; Meijer, 2006]. Today, the Mediterranean experiences evaporative losses ranging from about 0.4 to 1.2 m/yr [Rohling et al., 2015, and references therein], or approximately 0.03 to 0.1 Sv (1 Sv = 10^6 m^3/s). However, Atlantic inflow is much larger, at about 0.8 Sv [Tsimplis and Bryden, 2000]. The majority of inflow balances denser Mediterranean Outflow (MO) ($\sim$ 0.7 Sv) [Tsimplis and Bryden, 2000; Garcia-Lafuente et al., 2011], which is saltier and thus denser than Atlantic water due to the evaporative losses. A visualization of the change in the temporal evolution of the fluxes, ^{87}Sr/^{86}Sr, and salinity for the Sorbas Basin at $g = 12$ m^3/s per g/L is provided in Movie S1 in the supporting information.

4.3.3. Sensitivity of Salinity Parameters

Regardless of the initial salinity value selected, the Sorbas box salinity comes into dynamic equilibrium in less than 2 kyr (Figures 4b–4d). Mediterranean salinity does not affect the amplitude of the salinity response across a cycle. The results shown in Figure 4 are for a Mediterranean salinity of 37 g/L; adjusting Mediterranean salinity to 39 g/L shifts the salinity curves two units higher, but all other parameters remain the same, including lag times (Figures 4b–4d, star-marked shaded bars). Consequently, a wide range of Mediterranean salinity (~33 to 45 g/L) will satisfy the requirement that Sorbas Basin salinity remains within the tolerance of planktic foraminifera and results in the same relationship between the freshwater budget and Sr isotope ratio.

This result illustrates that major changes in salinity observed in marginal basins are driven by the salinity of the open Mediterranean basin, and is consistent with the accepted model of a deep Mediterranean basin during MSC Stage 1 (5.97–5.61 Ma [CIESM, 2008; Krijgsman and Meijer, 2008; Roveri et al., 2008; Manzi et al., 2013]). The onset of gypsum precipitation observed in marginal basins, which marks the onset of the MSC, is thought to be synchronous throughout the Mediterranean region on the scale of one precessional cycle [Krijgsman et al., 1999a, 2002]. Conversely, the box model results indicate salinity data obtained from marginal settings reflect salinity in the more inaccessible open Mediterranean. ^{87}Sr/^{86}Sr measured from the Primary Lower Evaporite (PLE) gypsum in Sorbas are within error of, or lower than, the global ocean curve [Lugli et al., 2010; Roveri et al., 2014; Evans et al., 2015; Reghizzi et al., 2017]. As the fluvial ^{87}Sr/^{86}Sr isotope signature in the Sorbas region continued to be higher than coeval ocean water values after the MSC (near or post 5.33 Ma; section 2.2), the oceanic and lower ^{87}Sr/^{86}Sr signatures found in Sorbas MSC Stage 1 PLE are consistent with a deep Mediterranean which maintained sea level above the Sorbas Basin connections.

4.3.4. Sensitivity to Depth Parameter

As indicated in section 4.2, the depth of the Sorbas Basin between 6.60 to 6.55 Ma was likely between 150 and 250 m, affecting the basin volume and thus potentially the box model results. Figures 4e and 4f show the results of the transient box model simulations for these depths. While the range of g increases with decreasing basin depth, the ranges of Q_R which can generate Sr isotope anomalies remain very similar (Table S2). Consequently, inferences regarding the hydrologic budget of the Sorbas Basin derived from our box model results are robust for basin depths from very shallow up to approximately 300 m. Additional results from this sensitivity study are provided in Text S3, Table S2, and Figures S2 and S3.

5. Discussion

5.1. Processes Affecting Seawater $^{87}Sr/^{86}Sr$ in Sorbas

The regular pattern of Sr anomalies observed, their temporal cyclicity, and relationship to lithology suggest precessional changes affected Sorbas Basin water. Precessional control on the basin has been observed in several studies, particularly in foraminiferal records [*Pérez-Folgado et al.*, 2003; *Sierro et al.*, 2003] (see also section 2.1 and Figure 2). Orbitally forced climate processes which could exert control on our record include eustatic sea level fluctuations impacting the Mediterranean-Sorbas gateway, river runoff or changes to the overall freshwater budget, and/or shifts in continental weathering regimes.

5.1.1. Eustatic Sea Level Change

The benthic foraminiferal assemblages and palaeogeographic reconstructions [*Braga and Martin*, 1996; *Esteban et al.*, 1996] indicate that the Sorbas Basin was shallow (150–250 m), with yet shallower, narrow, and relatively long connections to the western Mediterranean. The connections were not direct, but through the Vera Basin to the east, the Tabernas Basin to the west, and the Nijar Basin to the south (Figure 1). Thus, the connections were long and complex, consistent with the small values of g suggested by the box model, although the seawater $^{87}Sr/^{86}Sr$ observed over the majority of the interval studied indicate that ocean water entered the basin. Long, narrow, and/or shallow gateways are particularly sensitive to small changes in gateway size [*Simon and Meijer*, 2015] such as those that result from eustatic sea level variation. Eustacy certainly would have impacted the Sorbas-Mediterranean gateway as the Mediterranean was fully connected to the Atlantic prior to the MSC [*Roveri et al.*, 2014, and references therein]. At issue, then, is whether eustatic variation in sea level can modulate g to generate precessional changes in the Sr isotope record.

An important factor to address with respect to the numerical model is the use of constant volume. Small changes in sea level could impact significantly both basin volume and connectivity (g) due to the shallow, complex geometries of the basin and gateways. Although studies have linked changes in Antarctic ice volume to MSC onset [e.g., *Ohneiser et al.*, 2015], adequate records with the requisite temporal resolution on which to base sea level, and thus changes to basin volume or g for the interval considered here, are lacking. *Kouwenhoven et al.* [2003] indicate that no major sea level fluctuations are observed at open Mediterranean settings between ~8.2 and 6.5 Ma, although the methods used by those authors are not sensitive to changes on the order of a few tens of meters. For open ocean stable isotope records, obliquity strongly dominates eustatic sea level change in the Plio-Pleistocene [*Lisiecki and Raymo*, 2005; *Westerhold et al.*, 2005]. For some intervals of the late Miocene, some benthic foraminiferal $\delta^{18}O$ records appear to contain other orbital frequencies including precession (e.g., Ocean Drilling Program (ODP) Leg 154 Site 926, Ceara Rise, western equatorial Atlantic [*Shackleton and Hall*, 1997]; ODP Leg 162 Site 982 North Atlantic [*Hodell et al.*, 2001]; and ODP Site 659, Cape Verde, eastern equatorial Atlantic [*Colin et al.*, 2014]); unfortunately, these data sets tend to have relatively low resolution. One of the highest-resolution records available covering our interval is the Ceara Rise benthic foraminiferal $\delta^{18}O$ data set (Figure 2c) with an average of four samples per precessional cycle. For the interval considered here, Ceara Rise data show no obvious variation with either obliquity or precession, and no correlation with the Sorbas Basin Sr isotope data (Figure 2f), lithology, or faunal record (Figures 2d and 2e).

A reconstruction of sea level change within the Sorbas Basin has been performed for the Cariatiz reef section (Figure 1b) [*Sánchez-Almazo et al.*, 2007]; this section is located stratigraphically near the top of the UA marls, centered at approximately 6.34 Ma based on biostratigraphy. However, spectral analysis suggests that the sea level changes observed from this section likely occurred with obliquity, not precession [*Rodríguez-Tovar et al.*, 2013]. Consequently, while acknowledging that if eustatic sea level changes occurred, they will have

modified the Sorbas-Mediterranean gateway to some degree; we cannot currently attribute any of the systematic variation in the Sorbas Basin between 6.60 and 6.55 Ma to eustacy.

5.1.2. River Runoff

For river runoff to drive $^{87}Sr/^{86}Sr$ in the Sorbas Basin, an increase in Q_R would need to occur at the same orbital phase as the anomaly, i.e., near either precession minima or maxima (Figure 2). GCM simulations of late Miocene climate exhibit strong precessional shifts in the position of the Intertropical Convergence Zone [*Bosmans et al.*, 2015a; *Marzocchi et al.*, 2015], shifting the position of the North African monsoonal rain belt and causing related changes to river discharge into the Mediterranean [*Gladstone et al.*, 2007; *Bosmans et al.*, 2015b; *Marzocchi et al.*, 2015]. Maximum precipitation occurs during precession minima and reached the eastern Mediterranean via the Nile, as well as Miocene paleochannels, which flowed through modern-day Libya to the Gulf of Sirte draining a more humid Sahara [*Griffin*, 2002, 2011; *Paillou et al.*, 2009, 2012; *Ghoneim et al.*, 2012]. Enhanced runoff during precession minima dominates the Mediterranean's freshwater budget [*Marzocchi et al.*, 2016] and is consistent with spikes in productivity, water column stratification, and sapropel formation [e.g., *Rohling*, 1994; *Matthiesen and Haines*, 2003]. Were Mediterranean runoff the driver of the Sr anomalies observed, the $^{87}Sr/^{86}Sr$ excursion should therefore occur within the sapropelic layer, the layer associated temporally with precession minima, rather than within the diatomite and marl 2 layers as observed (Figure 2).

The GCM results indicate that in the western Mediterranean, maximum precipitation also occurs during precession minima. However, by comparison with the eastern basin, the variation in precipitation and river runoff between precession minima and maxima is less than half (Table S1), resulting from precessional shifts in a separate climate system originating over the Atlantic, known as winter storm tracks [*Kutzbach et al.*, 2014; *Toucanne et al.*, 2015]. This is consistent with relatively constant Al/Ti ratios in the four precessional cycles studied [*Filippelli et al.*, 2003]; in this context, changes in Al/Ti ratios would have indicated changes in river discharge recorded by changes in fluvially derived clays. Consequently, neither the timing nor the amplitude of local runoff variability are consistent with a direct Q_R control on the Sorbas Basin $^{87}Sr/^{86}Sr$.

The relationship between discharge rate and Sr concentration also precludes river runoff as the driving mechanism. Low discharge increases the time available to dissolve and incorporate ions into river water (e.g., Avon and Murchison, Australia; up to 1 mg/L [*Goldstein and Jacobsen*, 1987]) so that rivers draining arid regions tend to have relatively high Sr concentrations. Thus, higher Q_R should be associated with lower Sr concentrations, decreasing the potency of the fluvially derived Sr isotope signal (Figure 3a) and reducing its ability to generate an anomaly. Another potential driver related to variability in runoff is weathering; the Sr isotopic composition transferred from minerals to runoff or groundwater can vary with weathering intensity due to the preferential breakdown of Sr- and Rb-rich phases such as mica [e.g., *Nesbitt et al.*, 1980; *Blum and Erel*, 1997; *Li et al.*, 2007]. Again, because small variations in precipitation and river runoff are expected locally, shifts in weathering intensity are unlikely to explain the observations.

While the mass of Sr added to the basin by fluvial input per unit time is constant in the box model (i.e., constant Q_R), the only time that an anomaly occurs is during periods of significantly reduced exchange (Q_I, Q_O near 0; Figures 4b–4d). During these periods, the hydrologic budget of the basin is close to neutral, maintaining marginal basin salinity near that of the open Mediterranean and resulting in minimal density difference to drive exchange between the Mediterranean and Sorbas. Because there is negligible import of oceanic Sr to the Sorbas Basin under these conditions, and negligible export of riverine Sr, a buildup of river-derived Sr occurs in the Sorbas Basin which eventually produces a Sr isotope anomaly. As g is held constant during any one model run (Figures 4b–4d), the mechanism suppressing exchange is not controlled by a reduction in physical connectivity but driven by the local freshwater budget, which controls the density contrast.

5.2. The Freshwater Budget and Vertical Mixing

The freshwater budget of a basin partly controls stratification and vertical mixing. Increased surface water salinity caused by evaporation leads to increased surface density and water column destabilization. This process will occur when the freshwater budget becomes negative ($E > P + Q_R$), and vertical mixing increases as the freshwater budget becomes more negative. The box model provides no insights into water column structure as it assumes fully mixed conditions. However, considerable information about changes in stratification and vertical mixing can be inferred from Sorbas' lithological and faunal patterns, and summarized as follows:

1. The sapropelic layers, with preserved laminations and minimal benthic foraminifera counts, are thought to be deposited under stratified conditions which inhibited bottom water oxygenation and bioturbation [*Sierro et al.*, 2001, 2003].

2. Diatom blooms are linked to nutrient availability or upwelling; under such conditions in the Sorbas Basin, upwelling is most likely [*Filippelli et al.*, 2003; *Sierro et al.*, 2003]. Our box model predictions of small variations in Q_R are consistent, implying that changes to runoff are not sufficient to explain the observations.

3. The increase in benthic to planktic foraminifera ratio (B/P) suggests enhanced bottom water oxygenation coinciding with the homogeneous marls [*Pérez-Folgado et al.*, 2003]. Specifically, B/P increases through marl 1, peaks near or during the diatomite, and decreases through marl 2 back to near zero at the base of the sapropel (Figure 2d).

4. *Globigerina bulloides* is a planktic foraminifera species associated with cooler, more turbid upwelling waters [*Ortiz et al.*, 1995; *Pujol and Vergnaud Grazzini*, 1995]; this species does not bear symbionts, thus is adapted to lower light levels in the water column [*Ortiz et al.*, 1995]. The abundance of *G. bulloides* increases through marl 1 and peaks during or just after the diatomite.

Taken together, these factors indicate that strong vertical mixing was initiated during marl 1, reached a maximum either during diatomite deposition or the peak in *G. bulloides* abundance in marl 2, and decreased back to stratified conditions at the base of the sapropelic layers.

In detail, the relationship between the fauna and lithologies in the nonsapropelic layers is more complex (Figures 2d and 2e) probably as a result of biological feedback. Bioavailable phosphorus is at maximum throughout the nonsapropelic layers and particularly during the diatomite [*Filippelli et al.*, 2003]. This suggests that productivity was very high in the diatomite, potentially causing oxygen depletion in the bottom waters resulting from organic matter decomposition. The nutrient availability proxy, P/Ti, falls at the top of the diatomites, suggesting that the transition from diatomite to marl 2 may be controlled primarily by nutrient depletion in the upwelling waters rather than a decrease in the vigor of upwelling itself [*Filippelli et al.*, 2003]. *Globigerina bulloides* abundance may be affected by dust or other causes of turbidity in the water column, as well as temperature and food availability, and thus changes in its abundance may also be influenced by factors other than upwelling [*Ortiz et al.*, 1995; *Pujol and Vergnaud Grazzini*, 1995]. However, the general faunal pattern is consistent throughout the entire UA marl succession, not only the four cycles studied here (Figure 2), and supports most intense vertical mixing around or just after the time of diatomite deposition [*Sierro et al.*, 2003].

5.2.1. ^{87}Sr/^{86}Sr and Vertical Mixing

The Sr anomalies occur at the same time as the maximum in *G. bulloides* in all cycles (Figures 2e and 2f). This implies that the isotope anomaly was produced during strong vertical mixing of the water column, e.g., during the most negative part of the hydrologic cycle. This phase relationship is simulated in Figure 4b. In this case, the Sorbas Basin freshwater budget is positive except for a brief period when the freshwater budget becomes negative ($E > P + Q_R$), immediately preceding the Sr anomaly. This scenario is consistent with the phasing of water column stratification, as positive hydrologic budget conditions occur during sapropelic layer deposition. The case illustrated in Figure 4d, where Sorbas has a mostly negative freshwater budget, causes the Sr anomaly peaks to be out of phase by half a precessional cycle with the implied water column stratification. We conclude that in contrast with the negative late Miocene freshwater budget for the main Mediterranean basin, as indicated by several modeling studies [e.g., *Blanc*, 2000; *Ryan*, 2008; *Marzocchi et al.*, 2016], the Sorbas Basin likely had a primarily positive freshwater budget, based on the observed phase relationship between the Sr anomalies and faunal data.

Although the cycles studied here were deposited ~580 kyr before the onset of the MSC and deposition of Primary Lower Evaporites (PLE), the inference that the Sorbas Basin had a positive hydrologic budget is consistent with inferences for PLE at two locations including Sorbas. *Natalicchio et al.* [2014] found that the salinity of inclusions in gypsum from the Piedmont Basin (northwest Italy) is very low. In contrast, gypsum from the Conti Vecchi solar salt works (Sardinia, Italy), where seawater is evaporated to concentrate gypsum and halite as commercial products, has inclusions with high salinity, matching that of the precipitating brine. For Sorbas' PLE, *Evans et al.* [2015] observed δ^{34}S, δ^{18}O$_{SO4}$ and ^{87}Sr/^{86}Sr isotope signatures consistent with seawater, but δ^{18}O and δD values consistent with a freshwater source. A lower resolution, but longer-term, ^{87}Sr/^{86}Sr record including the first cycles of the Sorbas PLE gypsum shows similar precessional trends

[*Reghizzi et al.*, 2017]. This record confirms that the Sorbas Basin and western Mediterranean must have remained connected during deposition of both the Upper Abad marls and the MSC Stage 1 PLE, because the influence of the lower western Mediterranean ^{87}Sr/^{86}Sr end-member persisted within the Sorbas Basin. Thus, our model results provide a plausible hypothesis to explain the observations of *Natalicchio et al.* [2014] and *Evans et al.* [2015]: a positive freshwater budget over part of the precessional cycles may have led to incorporation of meteoric water within the gypsum.

5.2.2. Temporal Lags and Implications for Mediterranean Astronomical Tuning

The transient model results indicate that while changes in Sorbas salinity lag changes in its freshwater budget by ~1 kyr, the Sr peak lags changes in salinity by a similar interval (Figures 4b–4d, vertical bars). The lag between the Sr anomaly and salinity peak results from the time required to introduce enough riverine Sr to alter the basin isotopic composition while exchange between Sorbas and the Mediterranean is suppressed. Assuming maximum vertical mixing is synchronous with maximum salinity, this temporal relationship suggests that the Sr isotope anomaly should lag behind maximum vertical mixing of the water column by ~1 kyr and should lag the hydrologic budget peak by ~2 kyr. The time lag observed is within error of the 3.3 ± 2.6 kyr figure determined by *Topper and Meijer* [2015]. The larger mean lag time of *Topper and Meijer* [2015] is attributable to differences in model setup. Those authors used a two-box configuration in which a "marginal" box exchanges with a Mediterranean "deep" box, which then exchanges with the Atlantic. Both boxes evolve with precession, with a lag related to each connection.

Phase lags between climate, lithology, and climate proxies have implications for the appropriate location of astronomical tuning tie points within each orbital cycle. Previous research has suggested that tuning of the Abad marls by tying precession minima to the midpoint of sapropelic layers [e.g., *Krijgsman et al.*, 1999a] is incorrect as sapropelic layers were deposited during the transition to precession minima, rather than being centered symmetrically around it [*Pérez-Folgado et al.*, 2003]. The Sr anomalies are associated with enhanced vertical mixing during the deposition of diatomite and/or marl 2 (Figure 2) and just after maximum salinity (Figure 4b). This supports the suggestion that astronomical tuning of the Abad Marls can be achieved more accurately by tying the diatomite layers to precession maxima. These layers are much thinner than the sapropelic ones, providing a smaller error in terms of time, and thus may be more accurate for the Sorbas Basin at subprecessional resolution. Using diatomites as tie points has also been suggested for other Mediterranean successions (e.g., Tripoli Formation [*Hilgen and Krijgsman*, 1999]).

Changing tie points between sedimentary layers within a precessional cycle will not greatly affect MSC chronology (changes of a few kyr might be expected). However, millennial-scale temporal lags in parameters such as salinity and vertical mixing exist between marginal and deep basins. Thus, a thorough understanding of the synchronicity of deposition of marker beds (sapropels, diatomites) between locations requires millennial precision. As climate signals are archived within the sediments, and these sediments are themselves employed to generate the age models we use to understand climatic changes, improved temporal precision will enable a better understanding of climate feedback between the marginal and open Mediterranean deposits. This is most important for pre-Pliocene Mediterranean climate records, which currently rely solely on marginal deposits that are often isolated and spatially distant from each other.

6. Conclusions

The interval from 6.60 to 6.55 Ma in the Sorbas Basin Upper Abad marls, approximately 0.6 Myr prior to the Messinian Salinity Crisis, is characterized by regularly occurring ^{87}Sr/^{86}Sr anomalies higher than the coeval global ocean ^{87}Sr/^{86}Sr value. These anomalies vary in phase with precession, are consistent with the local continental Sr isotope signature, and occur within or immediately above the diatomite layers. The precessional frequency indicates a climate-driven mechanism for the record, in parallel with cyclical changes in sedimentation and fauna.

Numerical box modeling indicates that the Sr isotope anomalies are driven primarily by restriction of Sorbas' marine connection with the western Mediterranean. This restriction is not controlled by gateway size, but by precessional fluctuations in the freshwater budget, which modulates the Mediterranean-Sorbas density contrast. Both import of oceanic Sr and export of the local Sr signal are inhibited during minimal density contrast, enhancing the effect of riverine Sr relative to periods of active exchange. This mechanism has been overlooked in the interpretation of seawater Sr isotope signatures in marginal marine systems. The model

results also demonstrate that average Sorbas Basin salinity is controlled by Mediterranean salinity. This means that major changes in marginal basin salinity, such as the transition to gypsum precipitation at the onset of the MSC, reflect changes in the salinity of the main Mediterranean basin on the scale of a single precessional cycle. At subprecessional timescales, however, the timing of salinity change and hence the lithological response to salinity varies as a result of an individual marginal basin's freshwater budget and volume. This challenges the assumption that specific lithologies (e.g., sapropels) formed at precisely the same time throughout the Mediterranean and thus have implications for the precision achievable with astronomical tuning as well as aiding our understanding of the temporal relationships between similar deposits at different locations.

Given constraints on water column stratification and vertical mixing provided by sediment and fossil characteristics, only a mainly positive freshwater budget is able to generate the Sr anomaly in the Sorbas Basin with the observed pattern. In such a scenario, the freshwater budget becomes negative only briefly, immediately preceding a Sr anomaly (Figure 4b). This relationship between freshwater budget and Sr isotope anomaly ties the diatomite layer to insolation minima. Diatomites may therefore be a more accurate tie point for astronomical tuning in the Sorbas Basin than sapropelic layers. Finally, a net positive hydrologic budget over small marginal basins such as Sorbas could reconcile the apparent contradiction of gypsum deposition in environments dominated by freshwater inputs.

References

Albarede, F., and A. Michard (1987), Evidence for slowly changing ^{87}Sr/^{86}Sr in runoff from freshwater limestones of southern France, *Chem. Geol.*, *64*(1–2), 55–65, doi:10.1016/0009-2541(87)90151-3.

Alve, E., and J. W. Murray (1999), Marginal marine environments of the Skagerrak and Kattegat: A baseline study of living (stained) benthic foraminiferal ecology, *Palaeogeogr. Palaeoclimatol. Palaeoecol.*, *146*, 171–193, doi:10.1016/S0031-0182(98)00131-X.

Andersson, P. S., G. J. Wasserburg, J. Ingri, and M. C. Stordal (1994), Strontium, dissolved and particulate loads in fresh and brackish waters: The Baltic Sea and Mississippi Delta, *Earth Planet. Sci. Lett.*, *124*, 195–210, doi:10.1016/0012-821X(94)00062-X.

Aufgebauer, A., and T. McCann (2010), Messinian to Pliocene transition in the deep part of the Sorbas Basin, SE Spain—A new description of the depositional environment during the Messinian Salinity Crisis, *Neues Jahrb. Geol. Palaeontol., Abh.*, *259*(2), 177–195, doi:10.1127/0077-7749/2010/0112.

Baggley, K. A. (2000), The late Tortonian-early Messinian foraminiferal record of the Abad Member (Turre formation), Sorbas Basin, Almería, south-east Spain, *Palaeontology*, *43*(6), 1069–1112, doi:10.1111/1475-4983.00162.

Bahr, A., et al. (2015), Persistent monsoonal forcing of Mediterranean outflow water dynamics during the late Pleistocene, *Geology*, *43*(11), 951–954, doi:10.1130/G37013.1.

Baker, P. A., J. M. Gieskes, and H. Elderfield (1982), Diagenesis of carbonates in deep-sea sediments - evidence from Sr/Ca ratios and interstitial dissolved Sr data, *J. Sediment. Petrol.*, *52*(1), 71–82, doi:10.1306/212F7EE1-2B24-11D7-8648000102C1865D.

Barker, S., M. Greaves, and H. Elderfield (2003), A study of cleaning procedures used for foraminiferal Mg/Ca paleothermometry, *Geochem., Geophys., Geosyst.*, *4*(9), 8407, doi:10.1029/2003GC000559.

Beets, C. J., and M. J. De Ruig (1992), ^{87}Sr/^{86}Sr dating of coralline algal limestones and its implications for the tectono-stratigraphic evolution of the eastern Prebetic (Spain), *Sediment. Geol.*, *78*(3–4), 233–250, doi:10.1016/0037-0738(92)90022-J.

Benito, R., J. López-Ruiz, J. M. Cebriá, J. Hertogen, M. Doblas, R. Oyarzun, and D. Demaiffe (1999), Sr and O isotope constraints on source and crustal contamination in the high-K calc-alkaline and shoshonitic neogene volcanic rocks of SE Spain, *Lithos*, *46*(4), 773–802, doi:10.1016/S0024-4937(99)00003-1.

Betzler, C., J. C. Braga, J. M. Martín, I. M. Sánchez-Almazo, and S. Lindhorst (2006), Closure of a seaway: Stratigraphic record and facies (Guadix basin, southern Spain), *Int. J. Earth Sci.*, *95*(5), 903–910, doi:10.1007/s00531-006-0073-y.

Bijma, J., W. W. Faber, and C. Hemleben (1990), Temperature and salinity limits for growth and survival of some planktonic foraminifers in laboratory cultures, *J. Foraminiferal Res.*, *20*(2), 95–116, doi:10.2113/gsjfr.20.2.95.

Birck, J. L. (1986), Precision K-Rb-Sr isotopic analysis: Application to Rb-Sr chronology, *Chem. Geol.*, *56*, 73–83, doi:10.1016/0009-2541(86)90111-7.

Blanc, P. L. (2000), Of sills and straits: A quantitative assessment of the Messinian Salinity Crisis, *Deep Sea Res., Part I*, *47*(8), 1429–1460, doi:10.1016/S0967-0637(99)00113-2.

Blum, J. D., and Y. Erel (1997), Rb-Sr isotope systematics of a granitic soil chronosequence: The importance of biotite weathering, *Geochim. Cosmochim. Acta*, *61*(15), 3193–3204, doi:10.1016/S0016-7037(97)00148-8.

Blum, J. D., C. A. Gazis, A. D. Jacobson, and C. P. Chamberlain (1998), Carbonate versus silicate weathering in the Raikhot watershed within the High Himalayan Crystalline Series, *Geology*, *26*(5), 411–414, doi:10.1130/0091-7613(1998)026<0411:CVSWIT>2.3.CO.

Bosmans, J. H. C., S. S. Drijfhout, E. Tuenter, F. J. Hilgen, L. J. Lourens, and E. J. Rohling (2015a), Precession and obliquity forcing of the freshwater budget over the Mediterranean, *Quat. Sci. Rev.*, *123*, 16–30, doi:10.1016/j.quascirev.2015.06.008.

Bosmans, J. H. C., S. S. Drijfhout, E. Tuenter, F. J. Hilgen, and L. J. Lourens (2015b), Response of the North African summer monsoon to precession and obliquity forcings in the EC-Earth GCM, *Clim. Dyn.*, *44*(1–2), 279–297, doi:10.1007/s00382-014-2260-z.

Braga, J. C., and J. M. Martin (1996), Geometries of reef advance in response to relative sea-level changes in a Messinian (uppermost Miocene) fringing reef (Cariatiz reef, Sorbas Basin, SE Spain), *Sediment. Geol.*, *107*, 61–81, doi:10.1016/S0037-0738(96)00019-X.

Braga, J. C., J. M. Martin, and J. L. Wood (2001), Submarine lobes and feeder channels of redeposited, temperate carbonate and mixed siliciclastic-carbonate platform deposits (Vera Basin, Almeria, southern Spain), *Sedimentology*, *48*, 99–116, doi:10.1046/j.1365-3091.2001.00353.x.

Brass, G. W. (1976), The variation of the marine ^{87}Sr/^{86}Sr ratio during Phanerozoic time: Interpretation using a flux model, *Geochim. Cosmochim. Acta*, *40*, 721–730, doi:10.1016/0016-7037(76)90025-9.

Bryden, H. L., and T. H. Kinder (1991), Steady two-layer exchange through the Strait of Gibraltar, *Deep-Sea Res., Part A*, *38*, S445–S463, doi:10.1016/S0198-0149(12)80020-3.

Bryden, H. L., and H. M. Stommel (1984), Limiting processes that determine basic features of the circulation in the Mediterranean Sea, *Oceanol. Acta*, *7*(3), 289–296.

CIESM (2008), The Messinian Salinity Crisis from mega-deposits to microbiology - a consensus report, *No. 33 in CIESM Workshop Monographs*, edited by F. Briand, 168 pp.

Colin, C., et al. (2014), Late Miocene to early Pliocene climate variability off NW Africa (ODP Site 659), *Palaeogeogr. Palaeoclimatol. Palaeoecol.*, *401*, 81–95, doi:10.1016/j.palaeo.2014.02.015.

Conticelli, S., et al. (2009), Trace elements and Sr-Nd-Pb isotopes of K-rich, shoshonitic, and calc-alkaline magmatism of the western Mediterranean region: Genesis of ultrapotassic to calc-alkaline magmatic associations in a post-collisional geodynamic setting, *Lithos*, *107*(1–2), 68–92, doi:10.1016/j.lithos.2008.07.016.

Do Couto, D., C. Gumiaux, L. Jolivet, R. Augier, N. Lebret, N. Folcher, G. Jouannic, J.-P. Suc, and C. Gorini (2014), 3D modelling of the Sorbas Basin (Spain): New constraints on the Messinian erosional surface morphology, *Mar. Pet. Geol.*, 1–16, doi:10.1016/j.marpetgeo.2014.12.011.

Dorst, S., and J. Schönfeld (2013), Diversity of benthic foraminifera on the shelf and slope of the NE Atlantic: Analysis of data sets, *J. Foraminiferal Res.*, *43*, 238–254, doi:10.2113/gsjfr.43.3.238.

Dronkert, H. (1976), Late Miocene evaporites in the Sorbas Basin and adjoining areas, *Mem. Soc. Geol. Italy*, 341–361.

Duggen, S., K. Hoernle, A. Klügel, J. Geldmacher, M. Thirlwall, F. Hauff, D. Lowry, and N. Oates (2008), Geochemical zonation of the Miocene Alborán Basin volcanism (westernmost Mediterranean): Geodynamic implications, *Contrib. Mineral. Petrol.*, *156*, 577–593, doi:10.1007/s00410-008-0302-4.

Emeis, K. C., U. Struck, H. M. Schulz, R. Rosenberg, S. Bernasconi, H. Erlenkeuser, T. Sakamato, and F. Martinez-Ruiz (2000), Temperature and salinity variationsof Mediterranea Sea surface waters over the last 16,000 years from records of planktonic stable oxygen isotopes and alkenone unsaturation ratios, *Palaeogeogr. Palaeoclimatol. Palaeoecol.*, *158*, 259–280, doi:10.1016/S0031-0182(00)00053-5.

English, N. B., J. Quade, P. G. DeCelles, and C. N. Garzione (2000), Geologic control of Sr and major element chemistry in Himalayan rivers, Nepal, *Geochim. Cosmochim. Acta*, *64*(15), 2549–2566, doi:10.1016/S0016-7037(00)00379-3.

Esteban, M., J. C. Braga, J. Martin, and C. De Santisteban (1996), Western Mediterranean reef complexes, in *Models for Carbonate Stratigraphy from Miocene Reef Complexes of Mediterranean Regions*, *SEPM Concepts Sedimentol. Paleontol.*, vol. 5, pp. 55–72, SEPM, Society for Sedimentary Geology, Tulsa, Okla.

Evans, N. P., A. V. Turchyn, F. Gázquez, R. R. Bontognali, H. J. Chapman, and D. A. Hodell (2015), Coupled measurements of $\delta^{18}O$ and δD of hydration water and salinity of fluid inclusions in gypsum from the Messinian Yesares Member, Sorbas Basin (SE Spain), *Earth Planet. Sci. Lett.*, *430*, 499–510, doi:10.1016/j.epsl.2015.07.071.

Farrell, J. W., S. C. Clemens, and L. P. Gromet (1995), Improved chronostratigraphic reference curve of late Neogene seawater $^{87}Sr/^{86}Sr$, *Geology*, *23*(5), 403–406, doi:10.1130/0091-7613(1995)023<0403:ICRCOL>2.3.CO;2.

Fenton, M., S. Geiselhart, E. J. Rohling, and C. Hemleben (2000), Aplanktonic zones in the Red Sea, *Mar. Micropaleontol.*, *40*(3), 277–294, doi:10.1016/S0377-8398(00)00042-6.

Filippelli, G. M., F. J. Sierro, J. A. Flores, A. Vázquez, R. Utrilla, M. Pérez-Folgado, and J. C. Latimer (2003), A sediment-nutrient-oxygen feedback responsible for productivity variations in late Miocene sapropel sequences of the western Mediterranean, *Palaeogeogr. Palaeoclimatol. Palaeoecol.*, *190*, 335–348, doi:10.1016/S0031-0182(02)00613-2.

Flecker, R., and R. M. Ellam (1999), Distinguishing climatic and tectonic signals in the sedimentary successions of marginal basins using Sr isotopes: An example from the Messinian salinity crisis, eastern Mediterranean, *J. Geol. Soc. London*, *156*(4), 847–854, doi:10.1144/gsjgs.156.4.0847.

Flecker, R., and R. M. Ellam (2006), Identifying late Miocene episodes of connection and isolation in the Mediterranean–Paratethyan realm using Sr isotopes, *Sediment. Geol.*, *188–189*, 189–203, doi:10.1016/j.sedgeo.2006.03.005.

Flecker, R., R. M. Ellam, C. Muller, A. Poisson, A. Robertson, and J. Turner (1998), Application of Sr isotope stratigraphy and sedimentary analysis to the origin and evolution of the Neogene basins in the Isparta angle, southern Turkey, *Tectonophysics*, *298*, 83–101.

Flecker, R., S. de Villiers, and R. M. Ellam (2002), Modelling the effect of evaporation on the salinity - 87Sr/86Sr relationship in modern and ancient marginal-marine systems: The Mediterranean Messinian Salinity Crisis, *Earth Planet. Sci. Lett.*, *203*, 221–233, doi:10.1016/S0012-821X(02)00848-8.

Flecker, R., et al. (2015), Evolution of the Late Miocene Mediterranean-Atlantic gateways and their impact on regional and global environmental change, *Earth Sci. Rev.*, *150*, 365–392, doi:10.1016/j.earscirev.2015.08.007.

Fortuin, A. R., J. M. D. Kelling, and T. B. Roep (1995), The enigmatic Messinian-Pliocene section of Cuevas del Almanzora (Vera Basin, SE Spain) revisited—Erosional features and strontium isotope ages, *Sediment. Geol.*, *97*(3–4), 177–201, doi:10.1016/0037-0738(95)00009-W.

Garcia-Lafuente, J., A. Sanchez-Roman, C. Naranjo, and J. C. Sanchez-Garrido (2011), The very first transformation of the Mediterranean outflow in the Strait of Gibraltar, *J. Geophys. Res.*, *116*, C07010, doi:10.1029/2011JC006967.

Ghoneim, E., M. Benedetti, and F. El-Baz (2012), An integrated remote sensing and GIS analysis of the Kufrah Paleoriver, eastern Sahara, *Geomorphology*, *139–140*, 242–257, doi:10.1016/j.geomorph.2011.10.025.

Gladstone, R., R. Flecker, P. Valdes, D. Lunt, and P. Markwick (2007), The Mediterranean hydrologic budget from a late Miocene global climate simulation, *Palaeogeogr. Palaeoclimatol. Palaeoecol.*, *251*(2), 254–267, doi:10.1016/j.palaeo.2007.03.050.

Goldstein, S. J., and S. B. Jacobsen (1987), The Nd and Sr isotopic systematics of river-water dissolved material: Implications for the sources of Nd and Sr in seawater, *Chem. Geol.*, *66*, 245–272, doi:10.1016/0168-9622(87)90045-5.

Griffin, D. L. (2002), Aridity and humidity: Two aspects of the late Miocene climate of North Africa and the Mediterranean, *Palaeogeogr. Palaeoclimatol. Palaeoecol.*, *182*(1–2), 65–91, doi:10.1016/S0031-0182(01)00453-9.

Griffin, D. L. (2011), The late Neogene Sahabi rivers of the Sahara and the Hamadas of the eastern Libya-Chad border area, *Palaeogeogr. Palaeoclimatol. Palaeoecol.*, *309*(3–4), 176–185, doi:10.1016/j.palaeo.2011.05.007.

Hebeda, E. H., N. A. I. M. Boelrijk, H. N. A. Priem, E. A. T. Verdurmen, R. H. Vershure, and O. J. Simon (1980), Excess radiogenic Ar and undisturbed Rb-Sr systems in basic intrusives subjected to alpine metamorphism in southeastern Spain, *Earth Planet. Sci. Lett.*, *47*, 81–90, doi:10.1016/0012-821X(80)90106-5.

Henderson, G. M., D. J. Martel, R. K. O'Nions, and N. J. Shackleton (1994), Evolution of seawater $^{87}Sr/^{86}Sr$ over the last 400 ka: The absence of glacial/interglacial cycles, *Earth Planet. Sci. Lett.*, *128*, 643–651, doi:10.1016/0012-821X(94)90176-7.

Hilgen, F., K. Kuiper, W. Krijgsman, E. Snel, and E. van der Laan (2007), Astronomical tuning as the basis for high resolution chronostratigraphy: The intricate history of the Messinian Salinity Crisis, *Stratigraphy*, *4*(2–3), 231–238.

Hilgen, F. J., and W. Krijgsman (1999), Cyclostratigraphy and astrochronology of the Tripoli diatomite formation (pre-evaporite Messinian, Sicily, Italy), *Terra Nova*, *11*, 16–22, doi:10.1046/j.1365-3121.1999.00221.x.

Hillbrecht, H. (1996), Extant planktic foraminifera and the physical environment in the Atlantic and Indian Oceans: An atlas based on Climap and Levitus (1982) data, Zürich.

Van Hinsbergen, D. J. J., T. J. Kouwenhoven, and G. J. Van Der Zwaan (2005), Paleobathymetry in the backstripping procedure: Correction for oxygenation effects on depth estimates, *Palaeogeogr. Palaeoclimatol. Palaeoecol.*, *221*(3–4), 245–265, doi:10.1016/j.palaeo.2005.02.013.

Hodell, D. A., J. H. Curtis, F. J. Sierro, and M. E. Raymo (2001), Correlation of late Miocene to early Pliocene sequences between the Mediterranean and North Atlantic, *Paleoceanography*, *16*(2), 164–178, doi:10.1029/1999PA000487.

Hsü, K. J., W. B. F. Ryan, and M. B. Cita (1973), Late Miocene dessication of the Mediterranean, *Nature*, *242*, 240–244, doi:10.1038/242240a0.

Ingram, B. L., and D. J. Depaolo (1993), A 4300-year strontium isotope record of estuarine paleosalinity in San-Francisco Bay, California, *Earth Planet. Sci. Lett.*, *119*, 103–119, doi:10.1016/0012-821X(93)90009-X.

Jacobson, A. D., and J. D. Blum (2000), Ca/Sr and ^{87}Sr/^{86}Sr geochemistry of disseminated calcite in Himalayan silicate rocks from Nanga Parbat: Influence on river-water chemistry, *Geology*, *28*(5), 463–466, doi:10.1130/0091-7613(2000)28<463:SASGOD>2.0.CO;2.

de Jong, K. (2003), Very fast exhumation of high-pressure metamorphic rocks with excess ^{40}Ar and inherited ^{87}Sr, Betic Cordilleras, southern Spain, *Lithos*, *70*(3–4), 91–110, doi:10.1016/S0024-4937(03)00094-X.

Koho, K. A., and E. Piña-Ochoa (2012), Benthic foraminifera: Inhabitants of low-oxygen environments, in *Anoxia: Evidence for Eukaryote Survival and Paleontological Strategies*, edited by A. V. Altenbach, J. M. Bernhard, and J. Seckbach, pp. 249–285 , Springer, Netherlands.

Koho, K. A., E. Piña-Ochoa, E. Geslin, and N. Risgaard-Petersen (2011), Vertical migration, nitrate uptake and denitrification: Survival mechanisms of foraminifers (*Globobulimina turgida*) under low oxygen conditions, *FEMS Microbiol. Ecol.*, *75*(2), 273–283, doi:10.1111/j.1574-6941.2010.01010.x.

Kouwenhoven, T. J., F. J. Hilgen, and G. J. van der Zwaan (2003), Late Tortonian–early Messinian stepwise disruption of the Mediterranean–Atlantic connections: Constraints from benthic foraminiferal and geochemical data, *Palaeogeogr. Palaeoclimatol. Palaeoecol.*, *198*(3–4), 303–319, doi:10.1016/S0031-0182(03)00472-3.

Krijgsman, W., and P. T. Meijer (2008), Depositional environments of the Mediterranean "lower Evaporites" of the Messinian salinity crisis: Constraints from quantitative analyses, *Mar. Geol.*, *253*(3–4), 73–81, doi:10.1016/j.margeo.2008.04.010.

Krijgsman, W., F. J. Hilgen, I. Raffi, and F. J. Sierro (1999a), Chronology, causes and progression of the Messinian salinity crisis, *Nature*, *400*, doi:10.1038/2323.

Krijgsman, W., C. G. Langereis, W. J. Zachariasse, M. Boccaletti, G. Moratti, R. Gelati, S. Iaccarino, G. Papani, and G. Villa (1999b), Late Neogene evolution of the Taza – Guercif Basin (Rifian Corridor, Morocco) and implications for the Messinian salinity crisis, *Mar. Geol.*, *153*(1–4), 147–160, doi:10.1016/S0025-3227(98)00084-X.

Krijgsman, W., A. R. Fortuin, F. J. Hilgen, and F. J. Sierro (2001), Astrochronology for the Messinian Sorbas basin (SE Spain) and orbital (precessional) forcing for evaporite cyclicity, *Sediment. Geol.*, *140*(1–2), 43–60, doi:10.1016/S0037-0738(00)00171-8.

Krijgsman, W., M.-M. Blanc-Valleron, R. Flecker, F. J. Hilgen, T. J. Kouwenhoven, D. Merle, F. Orszag-Sperber, and J.-M. Rouchy (2002), The onset of the Messinian salinity crisis in the eastern Mediterranean (Pissouri Basin, Cyprus), *Earth Planet. Sci. Lett.*, *194*(3–4), 299–310, doi:10.1016/S0012-821X(01)00574-X.

Krijgsman, W., M. E. Leewis, M. Garcés, T. J. Kouwenhoven, K. F. Kuiper, and F. J. Sierro (2006), Tectonic control for evaporite formation in the eastern Betics (Tortonian; Spain), *Sediment. Geol.*, *188–189*, 155–170, doi:10.1016/j.sedgeo.2006.03.003.

Kutzbach, J. E., G. Chen, H. Cheng, R. L. Edwards, and Z. Liu (2014), Potential role of winter rainfall in explaining increased moisture in the Mediterranean and Middle East during periods of maximum orbitally-forced insolation seasonality, *Clim. Dyn.*, *42*, 1079–1095, doi:10.1007/s00382-013-1692-1.

Langlet, D., C. Baal, E. Geslin, E. Metzger, M. Zuschin, B. Riedel, N. Risgaard-Petersen, M. Stachowitsch, and F. J. Jorissen (2014), Foraminiferal species responses to in situ, experimentally induced anoxia in the Adriatic Sea, *Biogeosciences*, *11*(7), 1775–1797, doi:10.5194/bg-11-1775-2014.

Larrasoaña, J. C., A. P. Roberts, E. J. Rohling, M. Winklhofer, and R. Wehausen (2003), Three million years of monsoon variability over the northern Sahara, *Clim. Dyn.*, *21*(7–8), 689–698, doi:10.1007/s00382-003-0355-z.

Laskar, J., P. Robutel, F. Joutel, M. Gastineau, A. C. M. Correia, and B. Levrard (2004), A long-term numerical solution for the insolation quantities of the Earth, *Astron. Astrophys.*, *428*, 261–285, doi:10.1051/0004-6361:20041335.

Levitus, S., R. Burgett, and T. P. Boyer (1994), *World Ocean Atlas 1994. Volume 3 Salinity*, 99 pp., Natl. Environ. Satell., Data, and Inf. Serv. (NOAA), Washington, D. C.

Li, G., J. Chen, J. Ji, J. Liu, J. Yang, and X. Sheng (2007), Global cooling forced increase in marine strontium isotopic ratios: Importance of mica weathering and a kinetic approach, *Earth Planet. Sci. Lett.*, *254*(3–4), 303–312, doi:10.1016/j.epsl.2006.11.045.

Licari, L., and A. Mackensen (2005), Benthic foraminifera off West Africa (1°N to 32°S): Do live assemblages from the topmost sediment reliably record environmental variability? *Mar. Micropaleontol.*, *55*, 205–233, doi:10.1016/j.marmicro.2005.03.001.

Lisiecki, L. E., and M. E. Raymo (2005), A Pliocene-Pleistocene stack of 57 globally distributed benthic δ^{18}O records, *Paleoceanography*, *20*, PA1003, doi:10.1029/2004PA001071.

Lourens, L. J., A. Antonarakou, and F. J. Hilgen (1996), Evaluation of the Plio-Pleistocene astronomical timescale, *Paleoceanography*, *11*(4), 391–413, doi:10.1029/96PA01125.

Lourens, L. J., F. J. Hilgen, N. J. Shackleton, J. Laskar, and D. Wilson (2004), The Neogene period, in *A Geologic Time Scale*, edited by F. M. Gradstein, J. G. Ogg, and A. G. Smith, pp. 409–440, Cambridge Univ. Press, Cambridge, U. K., doi:10.1016/B978-0-444-59425-9.00029-9.

Lugli, S., V. Manzi, M. Roveri, and C. B. Schreiber (2010), The primary lower gypsum in the Mediterranean: A new facies interpretation for the first stage of the Messinian salinity crisis, *Palaeogeogr. Palaeoclimatol. Palaeoecol.*, *297*(1), 83–99, doi:10.1016/j.palaeo.2010.07.017.

Manzi, V., R. Gennari, F. Hilgen, W. Krijgsman, S. Lugli, M. Roveri, and F. J. Sierro (2013), Age refinement of the Messinian salinity crisis onset in the Mediterranean, *Terra Nov.*, 1–8, doi:10.1111/ter.12038.

Martin-Suarez, E., M. Freudenthal, W. Krijgsman, and A. R. Fortuin (2000), On the age of the continental deposits of the Zorreras member (Sorbas Basin, SE Spain), *Geobios*, *33*(4), 505–512, doi:10.1016/S0016-6995(00)80084-4.

Martin, E. E., N. J. Shackleton, J. C. Zachos, and B. P. Flower (1999), Orbitally-tuned Sr isotope chemostratigraphy for the late middle to late Miocene, *Paleoceanography*, *14*(1), 74–83.

Martín, J. M., and J. C. Braga (1994), Messinian events in the Sorbas Basin in southeastern Spain and their implications in the recent history of the Mediterranean, *Sediment. Geol.*, *90*(3–4), 257–268, doi:10.1016/0037-0738(94)90042-6.

Martín, J. M., J. C. Braga, and C. Betzler (2001), The Messinian Guadalhorce corridor: The last northern, Atlantic-Mediterranean gateway, *Terra Nova*, *13*(6), 418–424, doi:10.1046/j.1365-3121.2001.00376.x.

Martín, J. M., J. C. Braga, J. Aguirre, and Á. Puga-Bernabéu (2009), History and evolution of the North-Betic Strait (Prebetic zone, Betic Cordillera): A narrow, early Tortonian, tidal-dominated, Atlantic–Mediterranean marine passage, *Sediment. Geol.*, *216*(3–4), 80–90, doi:10.1016/j.sedgeo.2009.01.005.

Marzocchi, A., D. J. Lunt, R. Flecker, C. D. Bradshaw, A. Farnsworth, and F. J. Hilgen (2015), Orbital control on late Miocene climate and the North African monsoon: Insight from an ensemble of sub-precessional simulations, *Clim. Past*, *11*(10), 1271–1295, doi:10.5194/cp-11-1271-2015.

Marzocchi, A., R. Flecker, C. G. C. van Baak, D. J. Lunt, and W. Krijgsman (2016), Mediterranean outflow pump: An alternative mechanism for the Lago-Mare and the end of the Messinian Salinity Crisis, *Geology*, *44*(7), 523–526, doi:10.1130/G37646.1.

Mather, A. E. (2000), Adjustment of a drainage network to capture induced base-level change: An example from the Sorbas Basin, SE Spain, *Geomorphology*, *34*(3–4), 271–289, doi:10.1016/S0169-555X(00)00013-1.

Matthiesen, S., and K. Haines (2003), A hydraulic box model study of the Mediterranean response to postglacial sea-level rise, *Paleoceanography*, *18*(4), 1084, doi:10.1029/2003PA000880.

McArthur, J. M., D. Rio, F. Massari, D. Castradori, T. R. Bailey, M. Thirlwall, and S. Houghton (2006), A revised Pliocene record for marine-^{87}Sr/^{86}Sr used to date an interglacial event recorded in the Cockburn Island Formation, Antarctic Peninsula, *Palaeogeogr. Palaeoclimatol. Palaeoecol.*, *242*, 126–136, doi:10.1016/j.palaeo.2006.06.004.

McArthur, J. M., R. J. Howarth, and G. A. Shields (2012), Strontium isotope stratigraphy, in *The Geologic Time Scale 2012*, edited by F. M. Gradstein et al., pp. 127–144 , Elsevier B.V, Amsterdam.

McCulloch, M. T., and P. De Deckker (1989), Sr isotope constraints on the Mediterranean environment at the end of the Messinian salinity crisis, *Nature*, *342*, 62–65, doi:10.1038/342062a0.

McKenzie, J. A. (1999), From desert to deluge in the Mediterranean, *Nature*, *400*, 613–614, doi:10.1038/23131.

Meijer, P. T. (2006), A box model of the blocked-outflow scenario for the Messinian Salinity Crisis, *Earth Planet. Sci. Lett.*, *248*(1–2), 486–494, doi:10.1016/j.epsl.2006.06.013.

Melezhik, V. A., I. M. Gorokhov, A. B. Kuznetsov, and A. E. Fallick (2001), Chemostratigraphy of Neoproterozoic carbonates: Implications for "blind dating", *Terra Nova*, *13*, 1–11, doi:10.1046/j.1365-3121.2001.00318.x.

Millot, C. (1999), Circulation in the western Mediterranean Sea, *J. Mar. Syst.*, *20*(1–4), 423–442, doi:10.1016/S0924-7963(98)00078-5.

Mojtahid, M., F. Jorissen, B. Lansard, C. Fontanier, B. Bombled, and C. Rabouille (2009), Spatial distribution of live benthic foraminifera in the Rhône prodelta: Faunal response to a continental–marine organic matter gradient, *Mar. Micropaleontol.*, *70*, 177–200, doi:10.1016/j.marmicro.2008.12.006.

Montanari, A., B. Beaudoin, L. S. Chan, R. Coccioni, A. Deino, D. J. De Paolo, L. Emmanuel, E. Fornaciari, M. Kruge, and S. Lundblad (1997), Integrated stratigraphy of the middle and upper Miocene pelagic sequence of the Cònero Riviera (Marche region, Italy), in *Miocene Stratigraphy: An Integrated Approach*, vol. 15, edited by A. Montanari, G. Odin, and R. Coccioni, pp. 409–450 , Elsevier Science, Amsterdam.

Müller, D. W., and P. A. Mueller (1991), Origin and age of the Mediterranean Messinian evaporites: Implications from Sr isotopes, *Earth Planet. Sci. Lett.*, *107*(1), 1–12, doi:10.1016/0012-821X(91)90039-K.

Murat, A. (1999), 41. Pliocene-Pleistocene occurrence of sapropels in the western Mediterranean Sea and their relation to eastern Mediterranean Sapropels, in *Proceedings of the Ocean Drilling Program*, *Sci. Results*, vol. 161, edited by R. Zahn, M. C. Comas, and A. Klaus, pp. 519–527, Ocean Drilling Program, College Station, Tex.

Natalicchio, M., F. Dela Pierre, S. Lugli, T. K. Lowenstein, S. J. Feiner, S. Ferrando, V. Manzi, M. Roveri, and P. Clari (2014), Did late Miocene (Messinian) gypsum precipitate from evaporated marine brines? Insights from the Piedmont Basin (Italy), *Geology*, *42*(3), 179–182, doi:10.1130/G34986.1.

Nesbitt, H. W., G. Markovics, and R. C. Price (1980), Chemical processes affecting alkalies and alkaline earths during continental weathering, *Geochim. Cosmochim. Acta*, *44*, 1659–1666, doi:10.1016/0016-7037(80)90218-5.

Nier, A. O. (1938), The isotopic constitution of strontium, barium, bismuth, thallium and mercury, *Phys. Rev.*, *54*(4), 275–278.

Ohneiser, C., F. Florindo, P. Stocchi, A. P. Roberts, R. M. DeConto, and D. Pollard (2015), Antarctic glacio-eustatic contributions to late Miocene Mediterranean desiccation and reflooding, *Nat. Commun.*, *6*, 8765, doi:10.1038/ncomms9765.

Ortiz, J. D., A. C. Mix, and R. W. Collier (1995), Environmental control of living symbiotic and asymbiotic foraminifera of the California Current, *Paleoceanography*, *10*(6), 987–1009, doi:10.1029/95PA02088.

Paillou, P., M. Schuster, S. Tooth, T. Farr, A. Rosenqvist, S. Lopez, and J. M. Malezieux (2009), Mapping of a major paleodrainage system in eastern Libya using orbital imaging radar: The Kufrah River, *Earth Planet. Sci. Lett.*, *277*(3–4), 327–333, doi:10.1016/j.epsl.2008.10.029.

Paillou, P., S. Tooth, and S. Lopez (2012), The Kufrah paleodrainage system in Libya: A past connection to the Mediterranean Sea? *C. R. Geosci.*, *344*(8), 406–414, doi:10.1016/j.crte.2012.07.002.

Palmer, M. R., and J. M. Edmond (1989), The strontium isotope budget of the modern ocean, *Earth Planet. Sci. Lett.*, *92*, 11–26, doi:10.1016/0012-821X(89)90017-4.

Pérez-Folgado, M., F. J. Sierro, M. A. Bárcena, J. A. Flores, A. Vázquez, R. Utrilla, F. J. Hilgen, W. Krijgsman, and G. M. Filippelli (2003), Western versus eastern Mediterranean paleoceanographic response to astronomical forcing: A high-resolution microplankton study of precession-controlled sedimentary cycles during the Messinian, *Palaeogeogr. Palaeoclimatol. Palaeoecol.*, *190*, 317–334, doi:10.1016/S0031-0182(02)00612-0.

Poisson, A. M., J. L. Morel, J. Andrieux, M. Coulon, R. Wernli, and C. Guernet (1999), The origin and development of Neogene basins in the SE Betic Cordillera (SE Spain): A case study of the Tabernas-Sorbas and Huercal Overa basins, *J. Pet. Geol.*, *22*(1), 97–114, doi:10.1111/j.1747-5457.1999.tb00461.x.

Powell, J. L., and K. Bell (1970), Strontium isotopic studies of alkalic rocks: Localities from Australia, Spain, and the western United States, *Contrib. Mineral. Petrol.*, *27*, 1–10, doi:10.1007/BF00539537.

Pujol, C., and C. Vergnaud Grazzini (1995), Distribution patterns of live planktic foraminifers as related to regional hydrography and productive systems of the Mediterranean Sea, *Mar. Micropaleontol.*, *25*, 187–217, doi:10.1016/0377-8398(95)00002-I.

Pulido-Bosch, A. (1997), Los recursos hídricos de la Provincia de Almería, in *Actas del I y II Seminario del Agua*, edited by A. Pascual-Molina, pp. 65–89 , Instituto de Estudios Almerienses, Almeria, Spain.

Reghizzi, M., R. Gennari, E. Douville, S. Lugli, V. Manzi, P. Montagna, M. Roveri, F. J. Sierro, and M. Taviani (2017), Isotope stratigraphy (^{87}Sr/^{86}Sr, δ^{18}O, δ^{13}C) of the Sorbas basin (Betic Cordillera, Spain): Paleoceanographic evolution across the onset of the Messinian salinity crisis, *Palaeogeogr. Palaeoclimatol. Palaeoecol.*, *469*, 60–73, doi:10.1016/j.palaeo.2016.12.039.

Reinhardt, E. G., D. J. Stanley, and R. T. Patterson (1998), Strontium isotopic-paleontological method as a high-resolution paleosalinity tool for lagoonal environments, *Geology*, *26*(11), 1003–1006, doi:10.1130/0091-7613(1998)026<1003:SIPMAA>2.3.CO;2.

Richter, F. M., and Y. Liang (1993), The rate and consequences of Sr diagenesis in deep-sea carbonates, *Earth Planet. Sci. Lett.*, *117*(3–4), 553–565, doi:10.1016/0012-821X(93)90102-F.

Riding, R., J. Braga, J. Martín, and I. Sánchez-Almazo (1998), Mediterranean Messinian Salinity Crisis: Constraints from a coeval marginal basin, Sorbas, southeastern Spain, *Mar. Geol.*, *146*, 1–20, doi:10.1016/S0025-3227(97)00136-9.

De Rijk, S., F. J. Jorissen, E. J. Rohling, and S. R. Troelstra (2000), Organic flux control on bathymetric zonation of Mediterranean benthic foraminifera, *Mar. Micropaleontol.*, *40*, 151–166, doi:10.1016/S0377-8398(00)00037-2.

Rodríguez-Tovar, F. J., I. Sánchez-Almazo, E. Pardo-Igúzquiza, J. C. Braga, and J. M. Martín (2013), Incidence of obliquity and precession-forced Milankovitch cycles in the western Mediterranean: Early Messinian sedimentation in the Sorbas Basin (Almería, southern Spain), *Int. J. Earth Sci.*, doi:10.1007/s00531-013-0890-8.

Roep, T. B., and D. van Harten (1979), Sedimentological and ostracodological observations on Messinian post-evaporite deposits of some southeastern Spanish basins, *Ann. Geol. Pays Hell.*, *3*, 1037–1044.

Roep, T. B., C. J. Dabrio, A. R. Fortuin, and M. D. Polo (1998), Late highstand patterns of shifting and stepping coastal barriers and washover-fans (late Messinian, Sorbas Basin, SE Spain), *Sediment. Geol.*, *116*, 27–56, doi:10.1016/S0037-0738(97)00111-5.

Rohling, E. J. (1994), Review and new aspects concerning the formation of eastern Mediterranean sapropels, *Mar. Geol.*, *122*(1–2), 1–28, doi:10.1016/0025-3227(94)90202-X.

Rohling, E. J., G. Marino, and K. M. Grant (2015), Mediterranean climate and oceanography, and the periodic development of anoxic events (sapropels), *Earth-Sci. Rev.*, *143*, 62–97, doi:10.1016/j.earscirev.2015.01.008.

Rossignol-Strick, M. (1985), Mediterranean Quaternary sapropels, an immediate response of the African monsoon to variation of insolation, *Palaeogeogr. Palaeoclimatol. Palaeoecol.*, *49*(3–4), 237–263, doi:10.1016/0031-0182(85)90056-2.

Rossignol-Strick, M., and N. Planchais (1989), Climate patterns revealed by pollen and oxygen isotope records of a Tyrrhenian sea core, *Nature*, *342*, 413–416, doi:10.1038/342413a0.

Roveri, M., S. Lugli, V. Manzi, and B. C. Schreiber (2008), The Messinian Sicilian stratigraphy revisited: New insights for the Messinian salinity crisis, *Terra Nova*, *20*(6), 483–488, doi:10.1111/j.1365-3121.2008.00842.x.

Roveri, M., S. Lugli, V. Manzi, R. Gennari, and B. C. Schreiber (2014), High-resolution strontium isotope stratigraphy of the Messinian deep Mediterranean basins: Implications for marginal to central basins correlation, *Mar. Geol.*, *349*, 113–125, doi:10.1016/j.margeo.2014.01.002.

Ryan, W. B. F. (2008), Modeling the magnitude and timing of evaporative drawdown during the Messinian salinity crisis, *Stratigraphy*, *5*(3–4), 227–243.

Sanchez-Almazo, I. M., B. Spiro, J. C. Braga, and J. M. Martin (2001), Constraints of stable isotope signatures on the depositional palaeoenvironments of upper Miocene reef and temperate carbonates in the Sorbas Basin, SE Spain, *Palaeogeogr. Palaeoclimatol. Palaeoecol.*, *175*(1–4), 153–172, doi:10.1016/S0031-0182(01)00391-1.

Sánchez-Almazo, I. M., J. C. Braga, J. Dinarès-Turell, J. M. Martín, and B. Spiro (2007), Palaeoceanographic controls on reef deposition: The Messinian Cariatiz reef (Sorbas Basin, Almería, SE Spain), *Sedimentology*, *54*(3), 637–660, doi:10.1111/j.1365-3091.2006.00853.x.

Santisteban, C., and C. Taberner (1983), Shallow marine and continental conglomerates derived from coral reef complexes after desiccation of a deep marine basin: The Tortonian-Messinian deposits of the Fortuna Basin, SE Spain, *J. Geol. Soc. London*, *140*(3), 401–411, doi:10.1144/gsjgs.140.3.0401.

Schildgen, T., et al. (2014), Sea level and climate forcing of the Sr isotope composition of late Miocene Mediterranean marine basins, *Geochem., Geophys., Geosyst.*, *15*, 2964–2983, doi:10.1002/2014GC005332.

Schmiedl, G., A. Mackensen, and P. J. Müller (1997), Recent benthic foraminifera from the eastern South Atlantic Ocean: Dependence on food supply and water masses, *Mar. Micropaleontol.*, *32*, 239–287, doi:10.1016/S0377-8398(97)00023-6.

Shackleton, N. J., and M. A. Hall (1997), 24. The late Miocene stable isotope record, Site 926, in *Proceedings of the Ocean Drilling Program*, *Sci. Results*, vol. 154, edited by N. J. Shackleton, et al., pp. 367–373, Ocean Drilling Program, College Station, Tex., doi:10.2973/odp.proc.sr.154.119.1997.

Sierro, F. J., J. A. Flores, I. Zamarreno, A. Vazquez, R. Utrilla, G. Frances, F. J. Hilgen, and W. Krijgsman (1997), Astronomical cyclicity and sapropels in the pre-evaporitic Messinian of the Sorbas basin (western Mediterranean), *Geogaceta*, *21*, 199–202.

Sierro, F. J., J. A. Flores, I. Zamarreno, and A. Vazquez (1999), Messinian pre-evaporite sapropels and precession-induced oscillations in western Mediterranean climate, *Mar. Geol.*, *153*, 137–146.

Sierro, F. J., F. J. Hilgen, W. Krijgsman, and J. A. Flores (2001), The Abad composite (SE Spain): A Messinian reference section for the Mediterranean and the APTS, *Palaeogeogr. Palaeoclimatol. Palaeoecol.*, *168*(1–2), 141–169, doi:10.1016/S0031-0182(00)00253-4.

Sierro, F. J., J. A. Flores, G. Francés, A. Vazquez, R. Utrilla, I. Zamarreño, H. Erlenkeuser, and M. A. Barcena (2003), Orbitally-controlled oscillations in planktic communities and cyclic changes in western Mediterranean hydrography during the Messinian, *Palaeogeogr. Palaeoclimatol. Palaeoecol.*, *190*, 289–316, doi:10.1016/S0031-0182(02)00611-9.

Simon, D., and P. Meijer (2015), Dimensions of the Atlantic–Mediterranean connection that caused the Messinian Salinity Crisis, *Mar. Geol.*, *364*, 53–64, doi:10.1016/j.margeo.2015.02.004.

Sprovieri, M., M. Barbieri, A. Bellanca, and R. Neri (2003), Astronomical tuning of the Tortonian ^{87}Sr $/$ ^{86}Sr curve in the Mediterranean basin, *Terra Nova*, *15*, 29–35, doi:10.1046/j.1365-3121.2003.00446.x.

De Stigter, H. C., F. J. Jorissen, and G. J. Van der Zwaan (1998), Bathymetric distribution and microhabitat partitioning of live (Rose Bengal stained) benthic foraminifera along a shelf to deep sea transect in the southern Adriatic Sea, *Mar. Micropaleontol.*, *28*, 40–65.

Topper, R. P. M. (2013), A model analysis of atypical marine sedimentation in mediterranean basins, PhD thesis, Department of Earth Sciences, Utrecht Univ., Utrecht, The Netherlands.

Topper, R. P. M., and P. T. Meijer (2015), The precessional phase lag of Messinian gypsum deposition in Mediterranean marginal basins, *Palaeogeogr. Palaeoclimatol. Palaeoecol.*, *417*, 6–16, doi:10.1016/j.palaeo.2014.10.025.

Topper, R. P. M., R. Flecker, P. T. Meijer, and M. J. R. Wortel (2011), A box model of the late Miocene Mediterranean Sea: Implications from combined ^{87}Sr/^{86}Sr and salinity data, *Paleoceanography*, *26*, PA3223, doi:10.1029/2010PA002063.

Topper, R. P. M., S. Lugli, V. Manzi, M. Roveri, and P. T. Meijer (2014), Precessional control of Sr ratios in marginal basins during the Messinian salinity crisis? *Geochem., Geophys., Geosyst.*, *15*, 1926–1944, doi:10.1002/2013GC005192.

Toscani, L., G. Venturelli, M. Barbieri, S. Capedri, J. M. Fernandez Soler, and M. Oddone (1990), Geochemistry and petrogenesis of two-pyroxene andesites from Sierra de Gata (SE Spain), *Mineral. Petrol.*, *41*, 199–213, doi:10.1007/BF01168495.

Toucanne, S., C. M. Angue Minto'o, C. Fontanier, M.-A. Bassetti, S. J. Jorry, and G. Jouet (2015), Tracking rainfall in the northern Mediterranean borderlands during sapropel deposition, *Quat. Sci. Rev.*, *129*, 178–195, doi:10.1016/j.quascirev.2015.10.016.

Troelstra, S. R., H. M. van der Poel, C. H. A. Huisman, L. P. A. Geerlings, and H. Dronkert (1980), Paleoecological changes in the latest Miocene of the Sorbas Basin, SE Spain, *Géol. Méditerran.*, *7*, 115–126.

Tsimplis, M. N., and H. L. Bryden (2000), Estimation of the transports through the Strait of Gibraltar, *Deep Sea Res., Part I*, *47*(12), 2219–2242, doi:10.1016/S0967-0637(00)00024-8.

Vance, D., D. A. H. Teagle, and G. L. Foster (2009), Variable Quaternary chemical weathering fluxes and imbalances in marine geochemical budgets, *Nature*, *458*(7237), 493–496, doi:10.1038/nature07828.

Vázquez, A., R. Utrilla, I. Zamarreño, F. J. Sierro, J. A. Flores, G. Francés, and M. A. Bárcena (2000), Precession-related sapropelites of the Messinian Sorbas Basin (South Spain): Paleoenvironmental significance, *Palaeogeogr. Palaeoclimatol. Palaeoecol.*, *158*(3–4), 353–370, doi:10.1016/S0031-0182(00)00058-4.

Vazquez, M., A. Jabaloy, L. Barbero, and F. M. Stuart (2011), Deciphering tectonic- and erosion-driven exhumation of the Nevado-Filabride Complex (Betic Cordillera, southern Spain) by low temperature thermochronology, *Terra Nova*, *23*(4), 257–263, doi:10.1111/j.1365-3121.2011.01007.x.

Veizer, J. (1989), Strontium isotopes in seawater through time, *Annu. Rev. Earth Planet. Sci.*, *17*, 141–167, doi:10.1017/CBO9781107415324.004.

Voigt, J., E. C. Hathorne, M. Frank, H. Vollstaedt, and A. Eisenhauer (2015), Variability of carbonate diagenesis in equatorial Pacific sediments deduced from radiogenic and stable Sr isotopes, *Geochim. Cosmochim. Acta*, *148*, 360–377, doi:10.1016/j.gca.2014.10.001.

Weber, S. L., and E. Tuenter (2011), The impact of varying ice sheets and greenhouse gases on the intensity and timing of boreal summer monsoons, *Quat. Sci. Rev.*, *30*(3–4), 469–479, doi:10.1016/j.quascirev.2010.12.009.

Westerhold, T., T. Bickert, and U. Röhl (2005), Middle to late Miocene oxygen isotope stratigraphy of ODP site 1085 (SE Atlantic): New constrains on Miocene climate variability and sea-level fluctuations, *Palaeogeogr. Palaeoclimatol. Palaeoecol.*, *217*(3–4), 205–222, doi:10.1016/j.palaeo.2004.12.001.

Wright, R. (1978), Neogene benthic foraminifers from DSDP Leg 42A, Mediterranean Sea, in *Initial Reports of the Deep Sea Drilling Project*, vol. 42, Part 1, edited by K. J. Hsü et al., pp. 709–726, Ocean Drilling Program, College Station, Tex., doi:10.2973/dsdp.proc.42-1.1978.

Zeck, H. P., F. Albat, B. T. Hansen, L. R. Torres-Roldán, A. Garciá-Casco, and A. Martín-Algarra (1989), A 21 ± 2 Ma age for the termination of the ductile alpine deformation in the internal zone of the betic cordilleras, South Spain, *Tectonophysics*, *169*, 215–220, doi:10.1016/0040-1951(89)90196-0.

Van der Zwaan, G. J., F. J. Jorissen, and H. C. De Stigter (1990), The depth dependency of planktonic/benthic foraminiferal ratios: Constraints and applications, *Mar. Geol.*, *95*, 1–16, doi:10.1016/0025-3227(90)90016-D.